Journal of Computational Neuroscience (2019) 47:167–189
https://doi.org/10.1007/s10827-019-00731-7

Spontaneous synaptic drive in detrusor smooth muscle: computational investigation and implications for urinary bladder function

Nilapratim Sengupta [1] · Rohit Manchanda [1]

Received: 20 May 2019 / Revised: 9 September 2019 / Accepted: 16 September 2019 / Published online: 12 November 2019

Abstract
The detrusor, a key component of the urinary bladder wall, is a densely innervated syncytial smooth muscle tissue. Random spontaneous release of neurotransmitter at neuromuscular junctions (NMJs) in the detrusor gives rise to spontaneous excitatory junction potentials (SEJPs). These sub-threshold passive signals not only offer insights into the syncytial nature of the tissue, their spatio-temporal integration is critical to the generation of spontaneous neurogenic action potentials which lead to focal contractions during the filling phase of the bladder. Given the structural complexity and the contractile nature of the tissue, electrophysiological investigations on spatio-temporal integration of SEJPs in the detrusor are technically challenging. Here we report a biophysically constrained computational model of a detrusor syncytium overlaid with spatially distributed innervation, using which we explored salient features of the integration of SEJPs in the tissue and the key factors that contribute to this integration. We validated our model against experimental data, ascertaining that observations were congruent with theoretical predictions. With the help of comparative studies, we propose that the amplitude of the spatio-temporally integrated SEJP is most sensitive to the inter-cellular coupling strength in the detrusor, while frequency of observed events depends more strongly on innervation density. An experimentally testable prediction arising from our study is that spontaneous release frequency of neurotransmitter may be implicated in the generation of detrusor overactivity. Set against histological observations, we also conjecture possible changes in the electrical activity of the detrusor during pathology involving patchy denervation. Our model thus provides a physiologically realistic, heuristic framework to investigate the spread and integration of passive potentials in an innervated syncytial tissue under normal conditions and in pathophysiology.

Keywords Spatio-temporal integration · SEJP · Syncytium · Detrusor · Synaptic drive · Neurotransmission · Smooth muscle · Sub-threshold potentials · Urinary bladder · Computational model

1 Introduction

The urinary bladder is a vital component of the excretory system, assisting in the maintenance of water and electrolyte levels in the body. Micturition, the act of urine expulsion, is a key function of the bladder. The organ performs the crucial role of urine storage as well, during the phase of continence. The structural peculiarity of the bladder wall endows the organ with this dual functionality. However, the exact mechanisms underlying bladder function are poorly understood. Consequently, many aspects of bladder pathophysiology have remained obscure and treatment of bladder disorders lacks specificity and efficacy (Andersson et al. 2001; Wüst et al. 2002; Manchanda et al. 2019).

The smooth muscle layer of the bladder wall (the detrusor smooth muscle) endows it with contractile function. The detrusor has a bundled syncytial layout (Bramich and Brading 1996; Gabella 2012). While groups of cells form discrete bundles, communicating with each other through gap junctions (Neuhaus et al. 2002; Wang et al. 2006), individual bundles are likely to be electrically isolated (Brading 1997; Fry et al. 2004). Consequently, any electrical signal arising in a detrusor cell can propagate to interconnected neighbours within a bundle.

Action Editor: Upinder Singh Bhalla

✉ Rohit Manchanda
rmanch@iitb.ac.in

Nilapratim Sengupta
nilapratim@iitb.ac.in

[1] Department of Biosciences and Bioengineering, Indian Institute of Technology Bombay, Mumbai 400076, India

The detrusor receives a distributed innervation wherein the motor neurons branch out to form varicosities in apposition to the muscle cells (Drake et al. 2003; Gabella 2012). At these neuro-muscular junctions (NMJs), neurotransmitter release results in electrical activity in the post-junctional muscle cell (Bennett 1973; Manchanda et al. 2019). Physiologically, the neurotransmitter release may occur in two broad patterns, namely, a) in a coordinated fashion throughout the detrusor, as a result of action potential volleys propagating down the motor neurons, or b) asynchronously throughout the tissue due to stochastic release from varicosities. The former is known to mediate micturition *via* coordinated contraction of the bladder wall (Bramich and Brading 1996). In contrast, spontaneous asynchronous release events assist in the crucial functions of filling and storage. They lead to spontaneously occurring electrical signals in the detrusor which can either be sub-threshold (spontaneous excitatory junction potentials or SEJPs), or supra-threshold (spontaneous action potentials or sAPs). Spontaneous action potentials cause small, focal contractions of the bundles in the detrusor (Hashitani et al. 2004a, b), independent of one another, such contractions being termed micromotions (Drake et al. 2017). These micromotions help in rendering the bladder wall mechanically compliant during continence (Meng et al. 2008).

Intracellular electrical recordings of spontaneous activity in the detrusor exhibit substantial diversity in signal amplitudes, kinetics and mean frequency of occurrence (Bramich and Brading 1996; Hashitani et al. 2004a; Young et al. 2008; Sengupta et al. 2018). While spikes in neurons and in skeletal muscles comprise of more or less fixed waveforms, in the detrusor they exhibit diverse amplitudes and kinetics even when recorded from a single smooth muscle cell (Padmakumar et al. 2018). Such atypical behaviour as opposed to neuronal or skeletal muscle can be attributed to the interplay of several factors, the interplay being modulated by the structural characteristics of the detrusor. Owing to the syncytial nature of the detrusor, signals recorded intracellularly in any given cell of the tissue arise from the spatio-temporal integration (STI) of signals generated in the recorded cell as well as those generated in the surrounding, electrically coupled smooth muscle cells. Some of the important factors that determine the characteristics of integrated synaptic activity are the extent of coupling between cells, the degree of innervation, and the mean interval of release at a given NMJ. The extent of coupling between cells determines the degree of signal propagation and of its corollary, signal attenuation, and thus governs the characteristics of signal spread. Degree of innervation is a measure of NMJ density across a detrusor bundle. Mean inter-release interval is a measure of how frequently spontaneous release occurs at any NMJ.

While the roles that such factors play in determining the features of spatio-temporal integration can be conceptually envisaged, a qualitative and quantitative evaluation of their precise contributions cannot be arrived at without targeted studies on these questions. Thus far, the influence of any individual factor towards spatio-temporal integration in the detrusor has not yet been explored, either experimentally or computationally. Nor has interaction between these contributors been examined. On the experimental front, a key reason is that electrical recording from smooth muscle such as the detrusor using microelectrodes is technically challenging and is sparsely reported. Detrusor smooth muscle cells have a cross-sectional diameter of ~ 6 μm and are about 200 μm in length (Fry et al. 1999). Owing to the small diameter of the detrusor cells and the contractile nature of the tissue, it is difficult to probe individual cells and record their electrical activity over appreciable spans of time as the set-up is highly sensitive to mechanical vibrations (Manchanda 1995). In such a scenario as this, a robust computational model, constrained tightly by biophysical data, can offer a powerful means of exploring the characteristics of spatio-temporal integration of the neural drive to the detrusor.

We present here a biophysically detailed, multi-compartment model of a detrusor smooth muscle bundle endowed with physiologically realistic, spatio-temporally distributed neurotransmission, constructed with a view to addressing the above-mentioned questions. In a novel approach, we overlaid the muscle model with a spatially distributed innervation to explore key features of synaptic drive in the detrusor. We ensured the fidelity of the model to available experimental data pertaining to SEJP amplitudes and mean inter-event intervals, thus tightly constraining the model by physiological data and making for a biophysically realistic simulation framework. Key characteristics of signal integration in detrusor were studied. Using systematic variation of parameters, we checked for robustness of the model, seeing if simulation outcomes were congruent with theoretical expectations, and tuned the model accordingly. In case of observation being incongruent with pre-existing knowledge, as was encountered in the case of location-dependence of electrical activity, we hypothesized the underlying cause for the apparent contradiction and carried out appropriate simulations to test the same.

Having validated our model, we used it towards the purposes for which computational models are best suited, such as addressing open physiological questions, testing hypotheses pertaining to aspects of detrusor function and dysfunction, and making experimentally testable predictions for select, plausible situations. Thus, we addressed open questions pertaining to a particular type of bladder pathophysiology, involving denervation of detrusor bundles. This is a situation in which patches of the tissue lose innervation (Johnston et al. 2012; Drake et al. 2017), and is termed patchy denervation. Histological studies on detrusor samples affected by patchy denervation have been reported (Brading 2005). However, studies on corresponding electrical changes are absent. Since electrical activity is an essential precursor to the mechanical functioning of the tissue, in-depth knowhow of alterations in signal propagation in such a disorder merit investigation. We

hypothesized that with such anomalies present, the excitability of the tissue may get adversely affected. Loss of innervation is expected to result in a reduced occurrence of junction potentials, thereby lowering the probability of spike generation in the detrusor. Using our model, we simulated patchy denervation and tested our hypothesis. We also hypothesized that augmented innervation in an unaffected zone within the abnormal tissue (as reported in certain imaging studies, Brading 2005) might compensate for the lost innervation. Making use of our model, we tested this proposition.

Our results also allow us to put forth predictions relating to detrusor function that may be tested through experimental investigation. For instance, with the help of our model we show how mean frequency of spontaneous neurotransmitter release can affect signal integration in the detrusor. Our findings suggest that release frequencies at varicosities can be implicated in pathology pertaining to continence. This prediction from our model can be tested experimentally using drugs such as α-Latrotoxin (Krasnoperov et al. 1997; Young et al. 2008) that are known to influence neurotransmitter release from varicosities.

We present here our work directed towards understanding random spontaneous neurotransmitter action within a single bundle which eventually leads to the micromotion that underlies continence. We study how signals arising in spatially distributed different cells within a bundle integrate over time. We next explore the individual contributions of key parameters (innervation density, strength of coupling, mean interval of release at a varicosity) towards spatio-temporal integration of electrical signals in the detrusor. Subsequently we investigate how these factors interplay to modulate the electrical activity of the tissue when varied in combination. Furthermore, we use our model to test a hypothesis pertaining to possible changes in the electrical excitability of the tissue under a pathophysiological condition. Active ion channels, which give rise to action potentials, involve complex mechanisms that demand separate explorations. Since our focus was on delineating and analysing the spatio-temporal dynamics of spontaneous neurotransmitter release across the tissue, we restricted ourselves to extensively exploring the parameter space in the passive domain. Active ion channels were however incorporated for pilot studies in order to corroborate certain model predictions.

2 Methods

2.1 The model

We used the NEURON simulation environment for model development and virtual experiments. NEURON, a platform that allows development of compartmental models, is primarily used for modeling nerve cells and neural networks. However, smooth muscle cells exhibit similar excitable characteristics and underlying biophysical mechanisms, and we find that the NEURON framework lends itself well to building networks of detrusor smooth muscle cells (Appukuttan et al. 2015).

Syncytium of muscle cells We adopted the three-dimensional syncytial model of the detrusor (Appukuttan et al. 2015) to represent the smooth muscle bundle receiving the modeled synaptic drive. This base model consists of a 3 dimensional layout of cells, each cell connected *via* gap junctions to all immediate neighbors along the three axes. Gap junctions were modeled as low-resistance shunts allowing flow of charge between connected cells as a function of potential gradient. Unless otherwise specified, we used for our simulations a bundle with 5 cells along each axis (Neuhaus et al. 2002), totaling 125 cells in the syncytium. Figure 1 shows a schematic (not to scale) of the model.

Synaptic drive The prime focus of our work was to explore the spatio-temporal integration of passive potentials in a syncytial detrusor bundle following spontaneous neurotransmitter release. Since no prior model exists for the synaptic drive feeding into the syncytial network, this model was developed *ab initio*. A synapse or neuro-muscular junction (NMJ) in the detrusor comprises of an axonal varicosity containing neurotransmitter lying in close proximity to a muscle cell, the latter being endowed with neurotransmitter receptors and receptor-linked ion channels. Neurotransmitter molecules, once released from the varicosity either due to a propagating axonal spike or due to spontaneous exocytosis, bind to the post-junctional receptors, which undergo conformational changes allowing ionic flux across the muscle cell membrane. In order to realize a synapse or NMJ on a detrusor cell we implemented the mechanism as a parallel conductance change in the cell membrane, activated following an event of neurotransmitter release (Sengupta et al. 2015). The conductance change at each NMJ was configured such as to generate double exponential kinetics (refer Table 1): an exponential increase to peak conductance, which mimics the kinetics of neurotransmitter binding to receptors, followed by a relatively sluggish exponential decay which captures the time course of both the closing of the neurotransmitter-activated ion channels receptors and the gradual decay of neurotransmitter concentration in the junctional cleft between varicosity and muscle cell (Sengupta et al. 2018). The time constants of rise and decay were tuned to obtain a close match with experimentally recorded NMJ current kinetics (Inoue and Brading 1990).

Randomness in time In any detrusor cell with an NMJ, SEJPs arise due to release of neurotransmitter from the innervating varicosity or varicosities, and successive instants of release happen randomly in time. We therefore modeled release from each varicosity as a Poisson process where a 'release-event' in

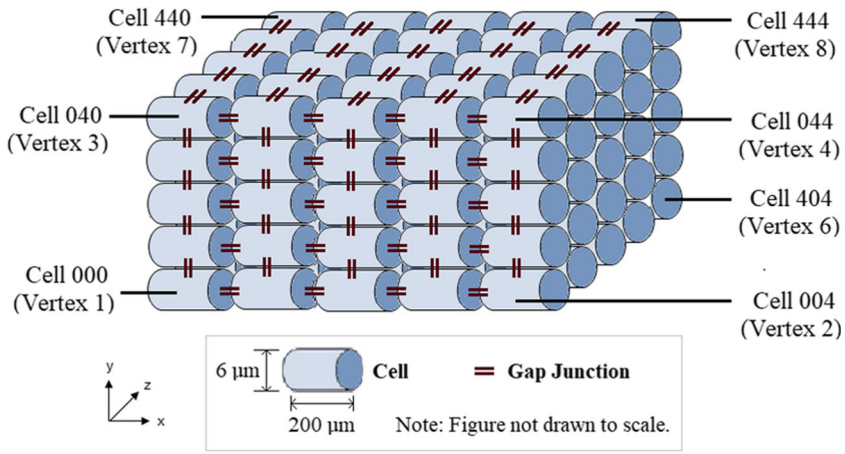

Fig. 1 Detrusor bundle schematic

a given time interval is independent of any other release(s) in the said interval. Consequently, inter-release intervals, when pooled, form a negative exponential distribution. Since our interest was to study the spread and interaction of SEJPs in a detrusor bundle, this facet was realized through NEURON's event based modelling approach. Over a given interval of time (duration of simulation) we used NEURON's NetStim class to generate a train of events ('release-events', event denoting spontaneous release of neurotransmitter), the interval between any two release-instants being drawn from a negative exponential distribution having a mean inter-release interval (IRI), thus satisfying the criterion of randomness in time. These 'release-events' were then delivered to the corresponding neurotransmitter-gated shunt representing the NMJ in the muscle membrane using NEURON's NetCon class. Each event thus mimicked release of neurotransmitter and elicited SEJPs distributed randomly in time.

Distribution in space As stated above, a detrusor bundle has a syncytial layout, with its network of smooth muscle cells receiving a spatially distributed innervation. Consequently, SEJPs are elicited not just randomly in time, but in space as well (at all the NMJs across the syncytium). In order to capture this aspect in our model, a train of events was delivered to each NMJ in the syncytium, with the individual mean IRI being different for the event train at each NMJ. Individual mean IRI for any given NMJ was selected from a normal distribution (network mean IRI and 5% standard deviation). The network mean IRI was obtained by tuning this value while validating the model against experimental data in terms of mean inter-event interval (in this case, "event" being an SEJP) or IEI (one of the outcome measures). To incorporate distributed NMJs (in cases where each cell is not endowed with an NMJ), the cells were first numbered from 1 through 125. Unique integral random numbers were generated between 1 and 125, the count depending on percentage of innervation (for example, 63 random numbers between 1 and 125 in case of 50% innervation). The cells having the corresponding numbers as identifiers were endowed with NMJs.

The key parameter values used in the passive model have been presented in Table 1.

Active ion channels for pilot studies The detrusor has a cohort of active ion channels that are responsible for generation of action potentials (Hayase et al. 2009). These include Ca^{2+} channels (L-type and T-type), Ca^{2+} activated K^+ channels (BK, IK, SK), voltage activated K^+ channels (KCNQ, Kv2), ATP activated K^+ channel, inward rectifying channel, *etc.* In-depth exploration of the effects of these ion channels on spatio-temporal integration in the detrusor merit an independent study. We incorporated these

Table 1 Key parameters and their values

Parameter		Value	Reference
Cell	Cell Length	200 µm	Appukuttan et al. 2015
	Cell Diameter	6 µm	
	Membrane Capacitance	1 µF/cm^2	
	Gap Junctional Resistance	30.6 MΩ	
	Intracellular Resistivity	181 Ω.cm	Fry et al. 1999
	Membrane Resistivity	138 kΩ.cm^2	
NMJ	Time Constant of Conductance Change	Rise 15 ms Decay 30 ms	Tuned to obtain a close match with experimentally recorded NMJ current kinetics (Inoue and Brading 1990).

ion channel models (Mahapatra et al. 2018) within our passive model, just for preliminary studies to corroborate predictions from our passive model with regard to excitability of the detrusor cells. Since intracellular Ca^{2+} dynamics are essential to the functioning of Ca^{2+} dependent ion channel mechanisms, a simple model of the same was also incorporated for these pilot studies (Mahapatra et al. 2018).

2.2 Outcome measures

Since our interest was to explore the effects of key parameters on spatio-temporal integration of SEJPs, we quantified and compared the results of our studies based on i) mean SEJP amplitude, ii) mean inter-event interval (IEI).

Mean SEJP amplitude was measured as the average value of all SEJP peak amplitudes, elicited at or propagated to the recorded cell. In the train of SEJPs recorded from a given cell, some were unitary SEJPs while others were compound (resulting from the superposition of two or more SEJPs). Amongst the range of spatio-temporal configurations of release explored here, a higher mean SEJP amplitude is taken to imply a greater probability of exceeding threshold and eliciting an active response (*i.e.*, a spike), and consequently a greater probability of the occurrence of spontaneous contraction.

Mean IEI is a measure of mean interval between two successive SEJPs (unitary or compound) recorded from a cell. Amongst the range of spatio-temporal configurations of release explored here, a higher mean IEI signifies a lower probability of superposition of signals, thus a lower probability of spike generation and consequently of spontaneous contraction.

2.3 Model tuning & validation

We worked with a 3 dimensional, cuboidal syncytial model of the detrusor of size 5^3, totalling 125 cells in the bundle (Neuhaus et al. 2002). Within the bundle, each cell was connected to its immediate neighbours by resistive shunts mimicking gap junctions, each endowed with a resistance of 30.6 MΩ. This value was arrived at (Appukuttan et al. 2015) by computing specific gap junctional resistance from the difference of total intracellular and cytoplasmic resistance.

Each cell in the bundle was endowed with an NMJ, thus overlaying an innervation of 100% (all cells innervated). Previous studies have reported extensive innervation in the detrusor (Gabella 1995; Bramich and Brading 1996). Since our model is the first of its kind to explore features of innervation and their effects on the electrical responses of the detrusor, we judged a 100% level of innervation to be a reasonable default value, given the findings of previous histological studies.

Mean frequency of spontaneous release from varicosities in the detrusor has not been reported experimentally. Prior studies have focused on the post-junctional effect by recording events from muscle cells (Hashitani et al. 2000; Hashitani et al. 2001; Young et al. 2008; Hayase et al. 2009). Given the syncytial nature of the detrusor, recorded activity from a muscle cell comprises of events elicited over the entire electrical network due to release from multiple varicosities. Post-junctional event frequency is thus not equivalent to release frequency from a single varicosity. Furthermore, prior focus has been greater on the sAPs rather than on the SEJPs, for which such time-domain data are scanty. We thus tuned our model in terms of the parameter 'mean IRI' so as to obtain physiologically relevant values for the outcome measures of our model. With a tuned value of 150 s for mean IRI, mean SEJP amplitude of 14.6 ± 0.6 mV was obtained. The corresponding mean IEI was 4.8 s. Experimental studies have reported amplitudes of SEJPs upto about 31.4 mV in guinea-pig detrusor (Bramich and Brading 1996). Also frequency of spontaneous activity has been observed in the range of 8–27 per minute, average frequency being 14.5 per minute (Hashitani et al. 2004a). Consequently, the experimentally observed average inter-event interval for spontaneous events in the guinea-pig detrusor is about 4.1 s. Thus the values for mean SEJP amplitude and inter-event interval, obtained from our simulations fall within the range of previously published values for these parameters, affirming that our model is rigorously constrained by physiological data.

Having tuned the parameters in the light of physiological data, we validated our model against functional features expected of it theoretically.

In a syncytial tissue, intracellular recording from any cell over time captures signals elicited within that cell, as well as those propagated from other interconnected cells in the bundle. In a given recording duration, SEJPs arising within the recorded cell are outnumbered by those that are elicited elsewhere. The SEJP elicited within the recorded cell suffers no attenuation due to inter-cellular propagation and is recorded at or almost at its full amplitude (allowing for a degree of attenuation arising from propagation within the cell). On the other hand, signals propagating from other cells suffer attenuation to differing degrees depending upon distance of travel (Tomita 1976). SEJPs originating in cells in closer proximity to the recorded cell have relatively higher amplitudes owing to lower levels of propagation-induced attenuation. SEJPs from cells farther away have even lower amplitudes because of severe attenuation in the course of propagation. The frequency of SEJPs originating in distant cells, however, is much greater, since cells further away from the recorded cell are markedly greater in number than near-neighbour cells. Thus, for individual SEJP amplitudes, *i.e.*, not considering superimposed signals, a negative exponential amplitude distribution is expected (Appukuttan et al. 2015). However, in the case of spatio-temporal integration, SEJPs are likely to superimpose. Consequently, extremely low-amplitude events diminish in frequency. As a result, the frequency histogram of SEJP amplitudes in a syncytial tissue in the case of spatio-temporal

integration has a right-skewed characteristic (Bramich and Brading 1996; Young et al. 2007). We verified these expectations for our simulated recordings (Fig. 2a).

Spontaneous release from any given varicosity is assumed to be independent of any prior release from the same or any other varicosity. As a result, corresponding SEJPs elicited throughout the detrusor are independent of one another. This is characteristic of a Poisson Process and thus, intervals between successive SEJPs form a negative exponential distribution. We verified the same for our simulated recordings (Fig. 2b).

3 Results

Having tuned and validated our computational model of the innervated detrusor syncytium in accordance with experimental data and theoretical predictions, as described above, we used it for a range of explorations to understand the spatio-temporal integration of signals following neurotransmission and the effect of various parameters that contribute to it. As outcome measures of spatio-temporal integration we analyzed: a) the mean amplitude of spontaneous excitatory junction potentials (SEJPs) and b) the mean inter-event interval (IEI) recorded from identified cells in the syncytium (see Methods).

3.1 Spatio-temporal integration (STI)

Owing to the syncytial nature of a smooth muscle bundle, SEJPs elicited in any innervated cell of the detrusor propagate electrically to other cells within the bundle. Also, at any innervated cell SEJPs are elicited randomly in time owing to stochastic spontaneous release from the varicosities. Consequently, intracellular recording from any cell in such an innervated bundle represents spatiotemporally integrated signals. Several studies, experimental and computational, have explored the summation in the somata of neurons of passive signals generated in their dendritic arbors (see, for instance, Cash and Yuste 1998; Cash and Yuste 1999; Poirazi et al. 2003). Estimation of linearity in signal superposition has been a key component of such investigations. Drawing a rough analogy between, on the one hand, the smooth muscle cell being recorded from and a neuronal soma, and on the other, the surrounding smooth muscle cells in the syncytium and the dendritic arbor, we wished to investigate analogously how signals arising in different regions of a detrusor bundle spread to and summate in the recorded cell.

For this study we placed one NMJ on the Vertex 1 cell or Cell 000 (refer Fig. 1, Methods) of a 5^3 detrusor bundle model. The second NMJ was placed in each case, on all the 125 cells in the syncytium. Of these, the following 5 cases were selected (based on the position of the second NMJ) to explore relative spatial distance from the Vertex 1 cell:

- Case I) Vertex 1 cell
- Case II) Vertex 3 cell, 4 cells away from Vertex 1 cell along the bundle height (y-axis)
- Case III) Centroidal cell, the cell being recorded from
- Case IV) Vertex 2 cell, 4 cells away from Vertex 1 cell along the bundle length (x-axis)
- Case V) Vertex 8 cell, 4 cells away from Vertex 1 cell along the bundle diagonal

In each case, the simulation protocol involved individual activation of the first NMJ, followed by individual activation of the second NMJ with sufficient delay in between to preclude any superposition of elicited SEJPs. Again following a sufficient delay, both the NMJs were simultaneously activated to record an integrated SEJP. In order to study the characteristics of summation, the peak amplitude of the integrated SEJP was compared against the algebraic sum of peak amplitudes of individuals SEJPs. We took 100% linearity as corresponding to the algebraic sum of the individual SEJPs.

Figure 3a depicts that in each of the aforementioned five Cases, the summation of SEJPs was sub-linear. However, the

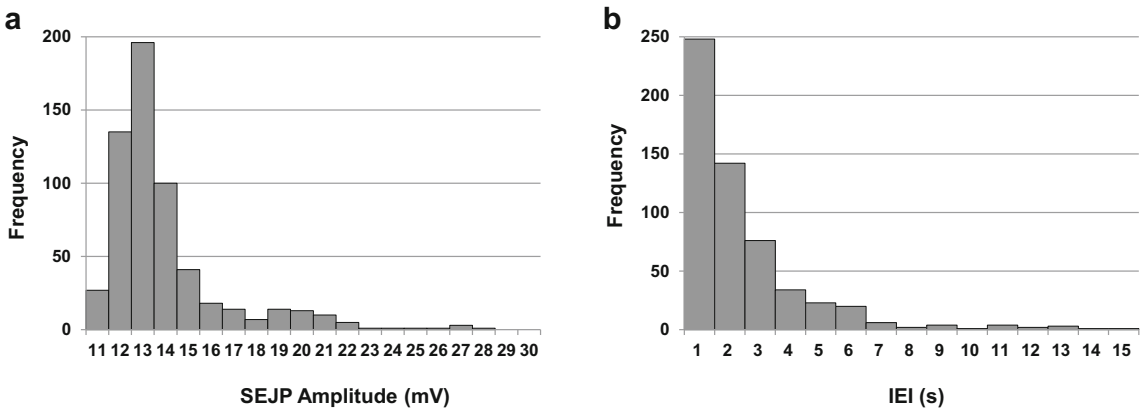

Fig. 2 (**a**) Frequency histogram of SEJP amplitudes, (**b**) Inter-event interval histogram of SEJPs

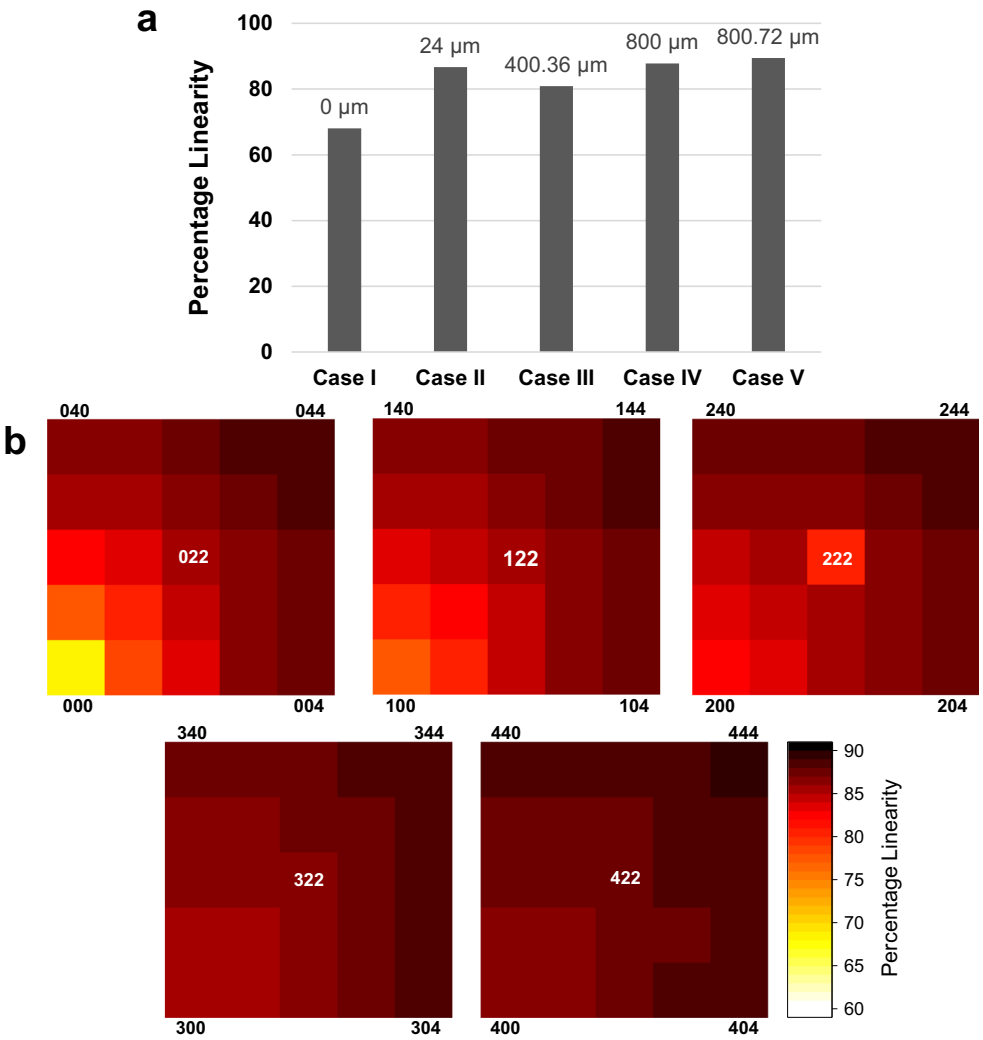

Fig. 3 Sub-linear spatio-temporal integration of SEJPs. (**a**) 5 specific cases (Labels denote distance between the two NMJs in each case). (**b**) Percentage linearity heat maps for all the 125 cells. Five heat maps are shown, one for each plane of the syncytium along the z-axis

degree of sub-linearity varied depending on the relative spatial location of NMJs in the detrusor bundle. The lowest percentage linearity (68.02%) was observed when both the SEJPs were elicited within the same cell, the distance between the two NMJs being 0 μm (Case I). Conversely, maximal percentage linearity (89.44%) was observed when the cells endowed with NMJs were farthest from each other (NMJs being 800.72 μm apart) at diametrically opposite vertices of the bundle (Case V). When the second NMJ was located on the centroidal cell, which was being recorded from (Case III), the observed percentage linearity was lower than expected in proportion to the distance involved.

Figure 3b presents percentage linearity heat maps of all the 125 cells in the syncytium. For clarity of visualization, the data have been presented in 5 slices, each slice having 25 cells corresponding to a plane along the thickness (z-axis) of the tissue. With increase in distance between the two NMJs, the percentage linearity of integrated SEJPs improved, as evidenced in the heat maps.

3.2 Effect of syncytium size

The network of interconnected cells in a syncytium allows current to dissipate into adjoining neighbours, thus reducing the effective input resistance. This affects the amplitude of individual electrical events (Tomita 1976). Accordingly, we investigated the manner and degree to which the size of such an electrical network affects spatio-temporal integration of SEJPs.

For this study, we carried out simulations over a range of syncytium sizes (5^3, 7^3, 9^3, 11^3, 13^3 and 15^3). We endowed the syncytia with 100% innervation (each smooth muscle cell receiving one NMJ) while recording from the centroidal cell in each case. At any given NMJ, we used a value for mean inter-release interval (IRI) drawn from a normal distribution (mean 150 s, s.d. ±5%). Gap junction resistance was uniform across the syncytia (30.6 MΩ).

Figure 4a shows that syncytium-size affects the mean amplitude of SEJPs recorded at the centroidal cell during spatio-temporal integration (STI) more, compared to the amplitude

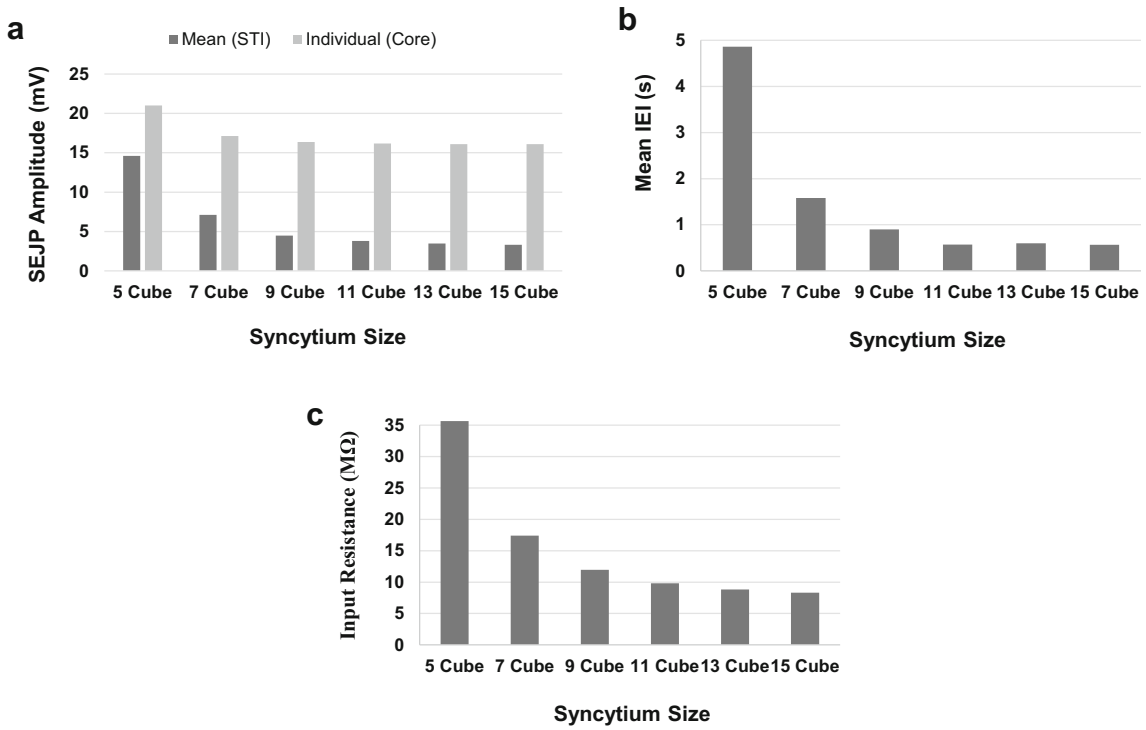

Fig. 4 Effect of syncytium size on (**a**) mean SEJP amplitude, (**b**) mean IEI, and (**c**) input resistance

of individual SEJP elicited at the centroidal cell. For example, as the size of the syncytium increases from 5^3 to 7^3, amplitude of single SEJP elicited at the centroidal cell falls by 18.44% whereas the mean SEJP amplitude of spatio-temporally integrated signals recorded from the same cell falls by 51.19%. As the size of a syncytium increases, a progressively greater number of cells get added to the network. This causes a reduction in input resistance (Fig. 4c) leading to reduced amplitude of individual SEJPs. Furthermore, in case of STI the cell recorded from receives signals propagated from increasingly distant cells. These propagated SEJPs undergo progressively heavier attenuation as a function of distance from the recording point. Both these factors contribute to the greater decrement in the mean amplitude of SEJPs being recorded during STI.

Figure 4b shows that with increase in syncytium size, the value of mean IEI falls as well. For example, as the size of the syncytium increases from 5^3 to 7^3, mean IEI declines by 68.27%. As more cells get added to the network, a greater number of NMJs get incorporated (since innervation density is fixed). Consequently, for a given mean release frequency a larger number of release events occur, thereby reducing the mean interval between consecutively recorded events.

3.3 Effect of coupling strength

While a larger syncytium provides greater scope for signal propagation, the extent of coupling between adjoining neighbours determines the degree of attenuation of propagating signals, thereby influencing the extent of propagation. We investigated the effect of strength of cell-to-cell coupling, as represented by gap junctional resistance, on spatio-temporal integration of signals.

For this study, we kept syncytium size invariant (5^3) and recorded from the centroidal cell in each case. Innervation density was retained at 100% and the value for mean IRI at each NMJ was drawn from a normal distribution (mean 150 s, s.d. ±5%). Gap junctional resistance was varied to values both lower than and greater than the default value (30.6 MΩ). We found the input resistance of a single detrusor cell to be 3.7 GΩ. Thus, in order to explore the condition of cells getting electrically isolated within the syncytium, an extremely high value of gap junctional resistance was required to be imposed.

Figure 5 shows the effect of intercellular coupling strength on mean SEJP amplitude and mean IEI along with representative simulation traces. Figure 5a shows fragments of membrane potential traces from simulations carried out with gap junctional resistances set at 10 MΩ, 30.6 MΩ and 100 MΩ. Figure 5b shows that current through gap junctions reduces to almost zero when gap junctional resistance is elevated to 74 GΩ, which is 20 times the input resistance of a single cell. Hence, we used this value of gap junctional resistance to mimic the situation of cells getting electrically isolated within the syncytium and the consequences of such isolation on signal integration. Figure 5c depicts that with rise in gap junctional resistance (reduced coupling), mean SEJP amplitude recorded from the centroidal cell falls, except for the case where cells are electrically isolated. Figure 5d shows that the mean IEI remains almost invariant with elevation of gap

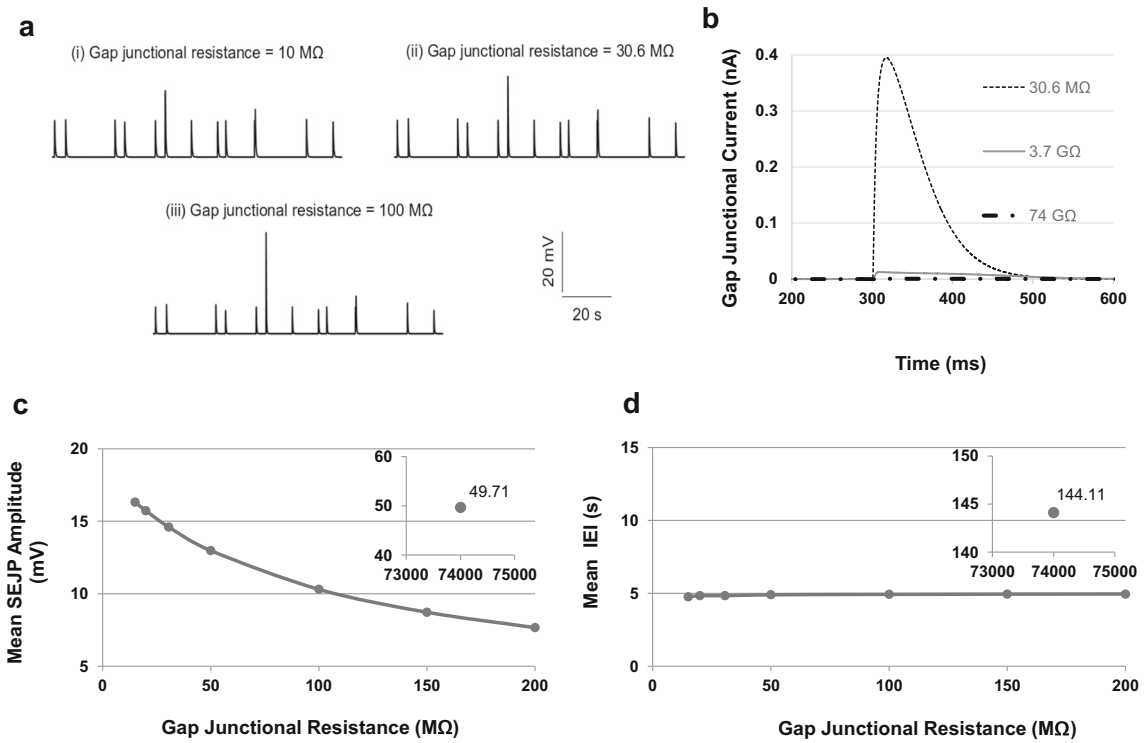

Fig. 5 Effect of coupling strength. (**a**) Representative simulation traces for the gap junctional resistances indicated. Effect of coupling strength on (**b**) gap junctional current, (**c**) mean SEJP amplitude, and (**d**) mean IEI. Inset graphs in (c) and (d) show respective values for 74 GΩ gap junctional resistance (mimicking electrical isolation of the cells)

junctional resistance, except when the cells are electrically isolated. The observations pertaining to the scenario of cells being isolated were outliers owing to the extremely high value of input resistance for an electrically isolated cell and hence, have been presented as insets in Fig. 5c, d.

3.4 Effect of innervation density

While the size of a syncytium and strength of coupling are critical in determining the spatial extent of an electrical sink for the generated signals, the density of innervation is a key factor governing the spatial distribution of spontaneous release in a network. We next explored how the density of innervation modulates spatio-temporal integration of SEJPs in the detrusor bundle. Towards this end, we carried out simulations in a 5^3 syncytial model. Gap junctional resistance was uniform throughout the syncytium (30.6 MΩ). Mean IRI at each NMJ was drawn from a normal distribution (mean 150 s, s.d. ±5%). The detrusor is reported to have a dense distributed innervation (Gabella 2012). We therefore explored innervation densities on either side of plausible physiological range, *i.e.*, 10%, 50% (by randomly selecting one-tenth and one-half of the cells, respectively, in the syncytium to be endowed with an NMJ), 100% (each cell receiving one NMJ), 150% (each cell receiving one NMJ and one-half of them receiving a second NMJ), 200% (every cell receiving 2 NMJs), 250% and 300%.

Figure 6 shows the effect of innervation density on mean SEJP amplitude and mean IEI along with characteristic simulation traces. Figure 6a shows fragments of membrane potential traces from simulations with innervation densities of 10%, 100% and 300%. Figure 6b shows that with increase in innervation density mean SEJP amplitude is elevated slightly. As more release sites (NMJs) get incorporated, more individual events are triggered, some of which superimpose and bring about an overall increase in amplitude of recorded signals. Figure 6c depicts the reduction in mean IEI with enhanced innervation density. With a larger number of release sites, and release at any given NMJ being spontaneous and random (*i.e.*, unaffected by release from any other site), the mean interval between any two subsequent SEJPs, whether elicited or propagated, diminishes when recorded from any given cell in the network.

3.5 Effect of mean inter-release interval

While degree of innervation determines spatial density of release sites, the temporal aspects of spontaneous release and its subsequent effect on signal integration are governed by frequency of release at any given NMJ. Thus, we examined the effect of mean IRI on signal integration in the detrusor syncytium. It is to be noted that while IRI is an independent parameter, governing the interval between successive releases at each NMJ, IEI is a dependent outcome measure, calculated

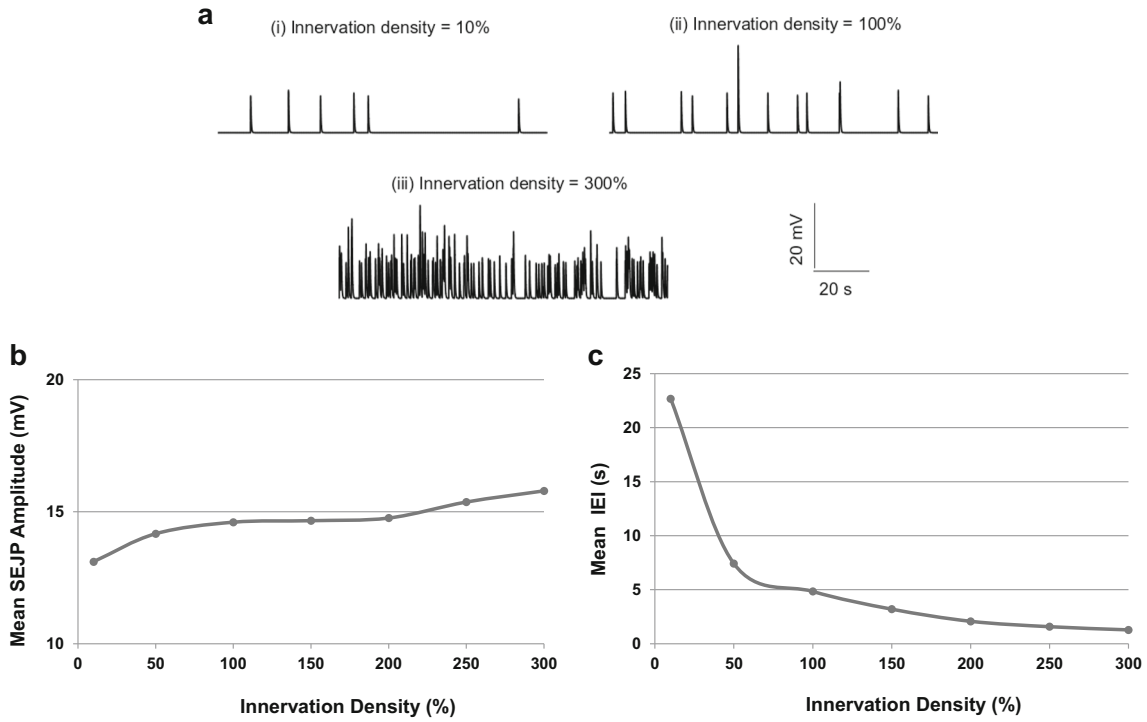

Fig. 6 Effect of innervation density. (**a**) Representative simulation traces for the innervation densities indicated. Effect of innervation density on (**b**) mean SEJP amplitude, (**c**) mean IEI

as the interval between two successive SEJPs recorded from a cell during simulation.

For this study, syncytium size was held constant (5^3) and gap junction resistance was uniform throughout the syncytium (30.6 MΩ). Each cell was endowed with one NMJ (100% innervation) and mean IRI at any given NMJ was drawn from a normal distribution with the mean differing in each case (s.d. ±5%).

Figure 7 shows the effect of mean IRI on mean SEJP amplitude and mean IEI along with typical simulation traces. Figure 7a shows fragments of membrane potential traces from simulations with mean IRIs of 50 s, 150 s and 250 s. Figure 7b depicts that with increase in mean IRI, mean SEJP amplitude reduces. Increased IRI results in events with greater temporal separation, thus allowing for a lower probability of superposition of successively occurring SEJPs. Figure 7c shows that with rise in mean IRI mean IEI increases. At the source, since the release is temporally sparse, elicited events occur after longer intervals.

3.6 Effect of recording location

Previous studies have reported that location of a cell in a syncytium can modulate its electrical response (Appukuttan et al. 2015). In order to test this idea using our model, we focused on two cell locations with distinct micro-environments, *viz.*, the cell at the edge/vertex of the syncytium, and the cell at its centroid, placed at the core of the bundle. We carried out simulations on 5^3 syncytial model with innervation density set to 100%. Gap junction resistance was invariant across the syncytium (30.6 MΩ) and mean IRI at each NMJ was selected from a normal distribution (mean 150 s, s.d. ±5%).

Figure 8 presents the effect of recording location within a syncytium on maximum and mean SEJP amplitudes and mean IEI. As may be noted from Fig. 8a, b, there is no appreciable difference in maximum or mean SEJP amplitude, maximum amplitude changing by just 0.95% and mean amplitude changing by 0.85%. Likewise, mean IEI did not change appreciably (0.74% difference) between both the locations. This observation is in contradiction to earlier reports of location within a syncytium affecting electrical response. We suspected that size of a syncytium might be a contributing factor in such a scenario. To test this hypothesis, the previous study was extended to include varying syncytial sizes.

In Fig. 8c the ratios of mean SEJP amplitudes recorded at the edge/vertex (Vertex 1) and at the corresponding centroidal cell have been plotted against syncytium size over the range indicated (5^3 to 15^3). The value of the ratio closest to 1 denotes that similar mean SEJP amplitudes were recorded at the edge and centroid cell of a 5^3 syncytium, as already observed in Fig. 8a. However, with increase in syncytium size, the mean amplitude of SEJPs recorded at any particular edge cell was found to progressively, and markedly, increment with respect to mean SEJP amplitudes recorded from corresponding centroid cells.

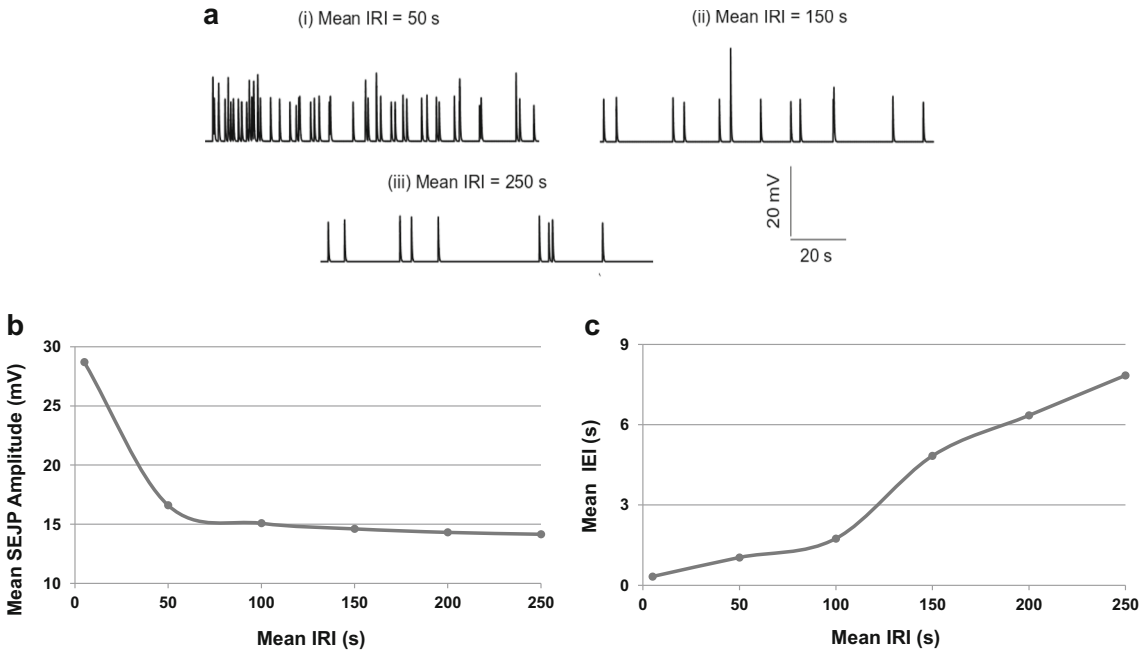

Fig. 7 Effect of mean IRI. (**a**) Representative simulation traces for the mean IRIs indicated. Effect of mean IRI on (**b**) mean SEJP amplitude, (**c**) mean IEI

3.7 Composite effects

The composite effect of location within a syncytium and its size, outlined previously, prompted us to explore interactions among the key factors that affect spatio-temporal integration of SEJPs in detrusor syncytium. In this group of studies, we kept one of the factors, *i.e.* syncytium size, constant (at a value of 5^3) as it has been reported that detrusor syncytium is composed of discrete bundles each of which comprises roughly of 100 cells (Neuhaus et al. 2002).

In the first set, mean IRI was varied between 5 s and 250 s (6 values) while density of innervation was varied between

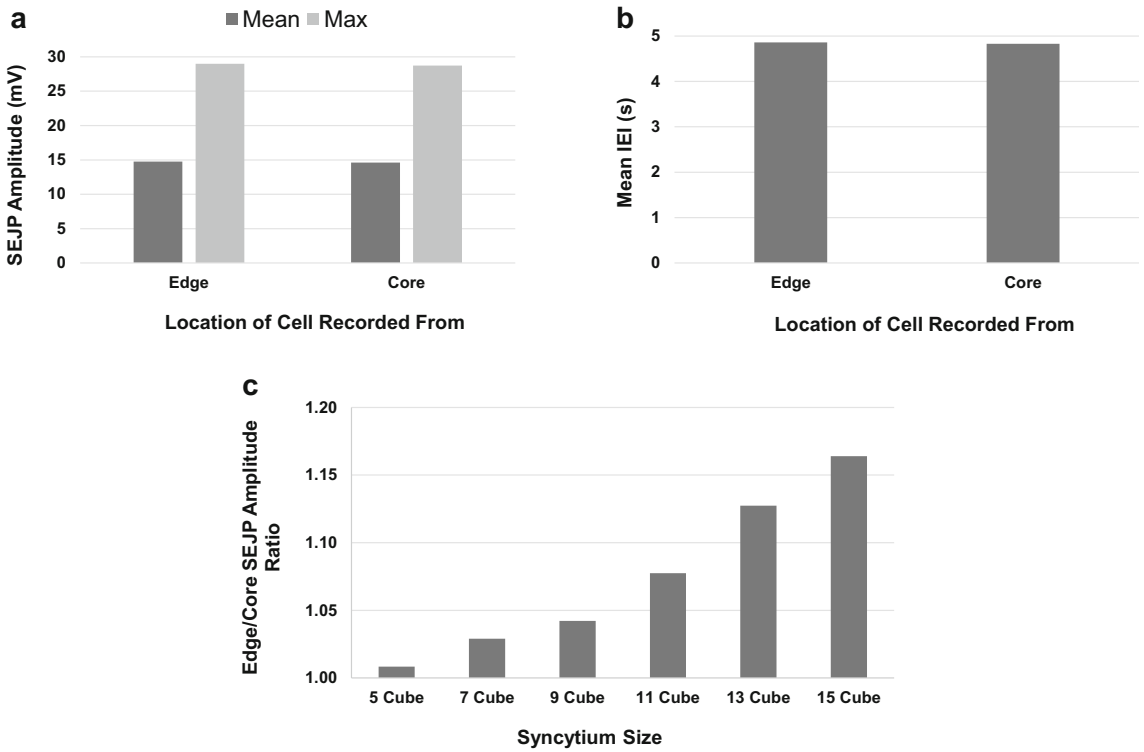

Fig. 8 Effect of recording location on (**a**) mean SEJP amplitude, and (**b**) mean IEI. (**c**) Ratio of mean SEJP amplitudes recorded at an edge and centroid cell – varying with syncytium size

10% and 300% (7 values). The gap junction resistance was kept fixed at 30.6 MΩ. In all simulations, recordings were made from the centroidal cell.

Figure 9 shows joint effects of innervation density and mean IRI on a) mean SEJP amplitude, and b) mean IEI. From Fig. 9a it is evident that SEJPs vary much more strongly with IRI than with innervation density. For any given value of mean IRI (particularly around values in the physiologically plausible range), mean SEJP amplitude shows smaller degrees of change with change in innervation density. In Fig. 9b we observe that the variable of interest, mean IEI, is more sensitive to innervation density than it is to mean IRI. For higher values of innervation density, mean IEI shows very little dependence on mean IRI.

In the next set of studies, coupling strength was varied incrementally in terms of gap junctional resistance (8 values) while density of innervation was varied between 10% and 300% (7 values). The mean IRI was kept fixed at 150 s. In all simulations, outputs were taken from the centroid cell.

Figure 10 shows the interaction between innervation density and coupling strength in determining a) mean SEJP amplitude and b) mean IEI. From Fig. 10a it is evident that mean SEJP amplitude is a stronger function of gap junctional resistance than of innervation density. From Fig. 10b we conclude that the mean inter-event interval is insensitive to change in strength of coupling for any given density of innervation. Thus, mean IEI is much more sensitive to innervation density than it is to coupling strength in a syncytium, except over very low innervation densities. Figure 10c, d reproduce the data presented in Fig. 10a, b respectively, with the incorporation of data pertaining to gap junctional resistance of 74 GΩ, where cells in the syncytium are effectively electrically isolated from each other.

Figure 11 shows the conjoint effect of mean IRI and coupling strength on a) mean SEJP amplitude, and b) mean IEI. In Fig. 11a it is observable that mean SEJP amplitude varies more strongly with gap junctional resistance than with mean IRI. In Fig. 11b we observe that mean IEI is insensitive to changes in gap junction resistance for any given value of mean IRI. Thus, mean IRI has a greater effect on mean IEI than does coupling strength in a syncytium. Figure 11c, d reproduce the data presented in Fig. 11a, b respectively, with the incorporation of data pertaining to gap junctional resistance of 74 GΩ, where cells in the syncytium are effectively electrically isolated from each other.

3.8 Study on denervation

As mentioned above, density of innervation appears to be a key factor in modulating the electrical response of the detrusor syncytium. Pathological conditions have been reported (Drake et al.

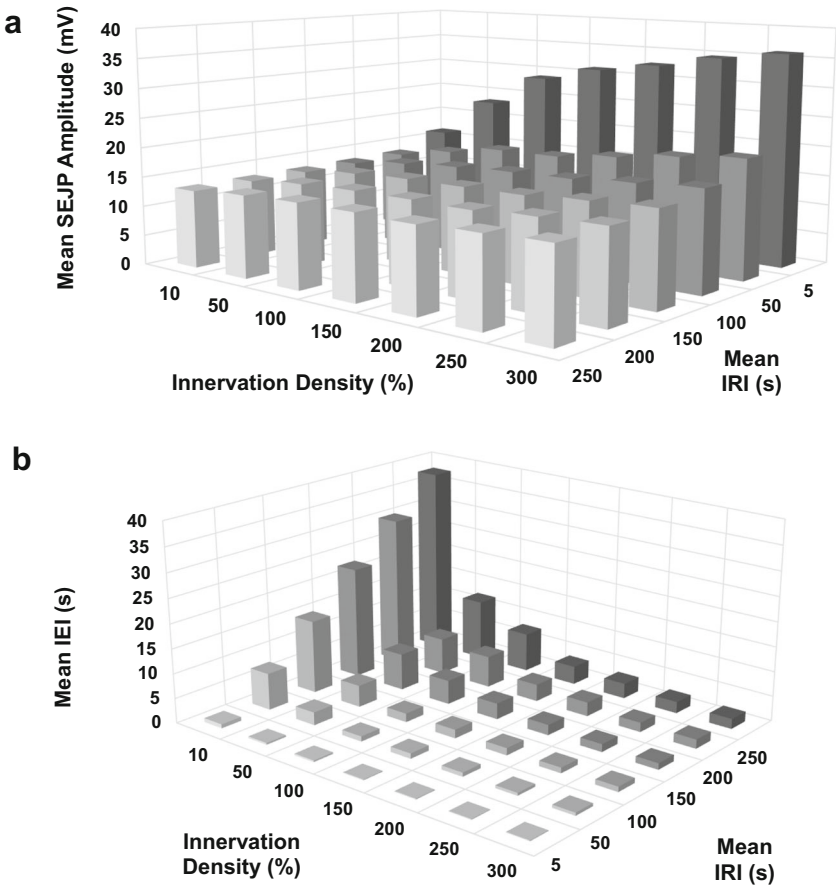

Fig. 9 Composite effect of innervation density and mean IRI on **a** mean SEJP amplitude, and **b** mean IEI

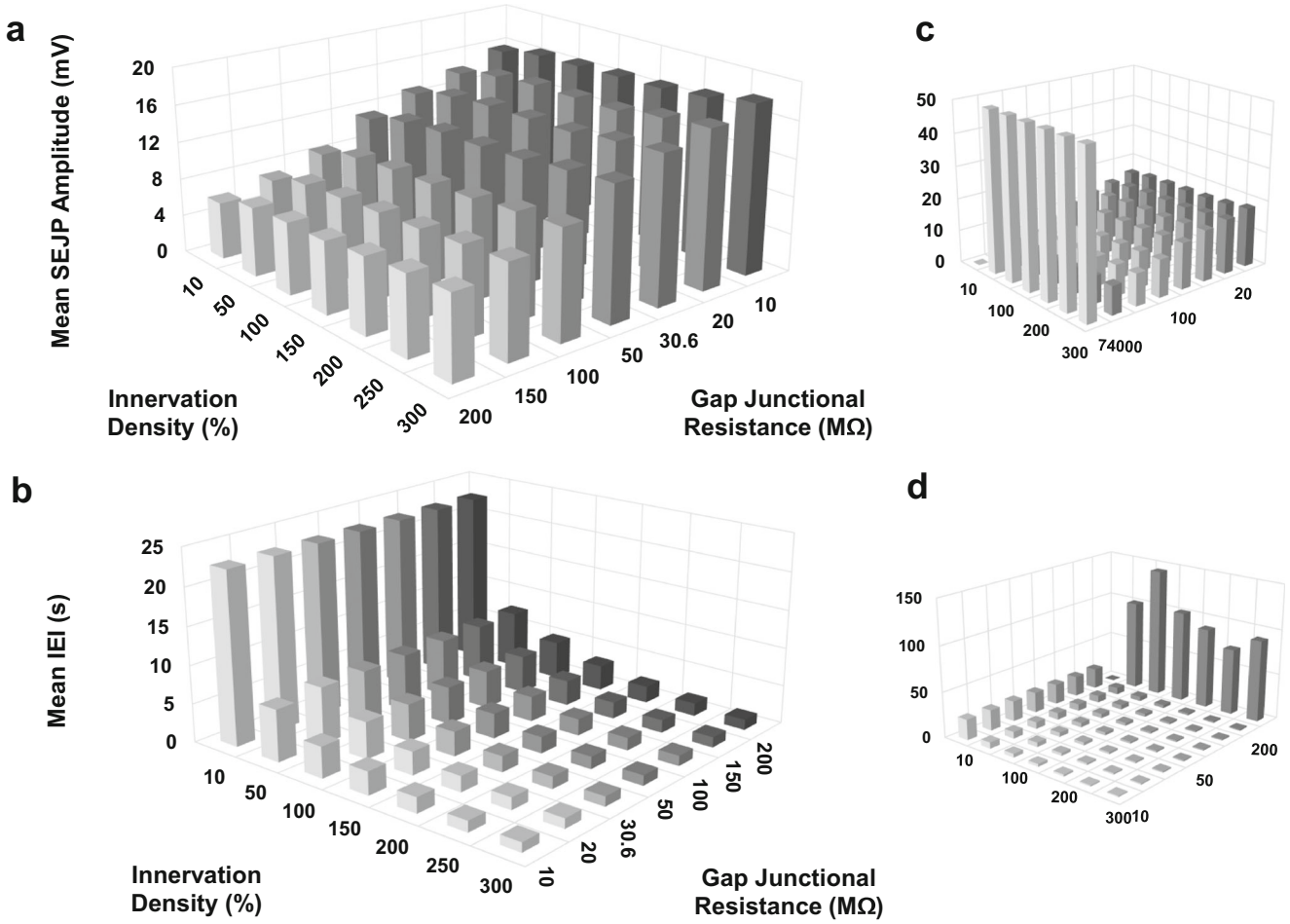

Fig. 10 Composite effect of innervation density and coupling strength on (**a**) mean SEJP amplitude, and (**b**) mean IEI. (**c**) and (**d**) are modified versions of (a) and (b) respectively, incorporating gap junctional resistance of 74 GΩ. This very large value of gap junctional resistance (mimicking electrical isolation of the cells) leads to the very high observed values of mean SEJP amplitudes and IEI, dwarfing the values presented in (a) and (b)

2017) in which a loss of innervation can impair the normal function of the bladder. Patchy denervation has been reported in histological studies (Brading 2005) wherein a certain portion of an otherwise healthy detrusor muscle loses its innervation. However, electrophysiological studies on such tissues are scarce. While it can readily be envisaged that such compromised innervation would alter the excitability of the affected bundle, the quantitative features of the altered excitability are difficult to predict, and we used our model to explore this question.

For this study we used a 5^3 syncytial model with spatially uniform gap junctional resistance of 30.6 MΩ. The mean IRI at any NMJ was drawn from a normal distribution (mean 150 s, s.d. ±5%). We simulated situations of denervation of increasing severity. In two different cases, 50% and 25% levels of innervation were retained by deactivating remaining NMJs. The exclusion of NMJs was carried out in well-defined regions in each case, thus mimicking patchy (and not random) denervation. We defined regions of denervation as follows. To simulate 50% denervation, NMJs on half of the cells from the third plane and all cells from the fourth and fifth planes of the syncytium along the z-axis were deactivated. To simulate the more severe scenario where only 25% of cells retain innervation, only the NMJs on all the 25 cells of the first plane and 7 cells from the second plane along the z-axis of the syncytium were retained.

Histological studies have reported patchily denervated bundles that exhibit an increase in innervation in the unaffected zone, possibly as a compensatory mechanism (Brading 2005). To test this possibility, the aforementioned simulations were repeated by doubling the innervation in unaffected regions. During each simulation we recorded the electrical activity from three cells – cell A (located in the central part of the unaffected region in the bundle), cell B (located in the central part of the denervated patch in the bundle) and cell C (located at the borderline region between unaffected and denervated regions). Thus, for each degree of denervation, we explored 6 distinctly different cellular microenvironments, as described and titled below.

1. Cell from unaffected region with regular innervation: Patchy-A

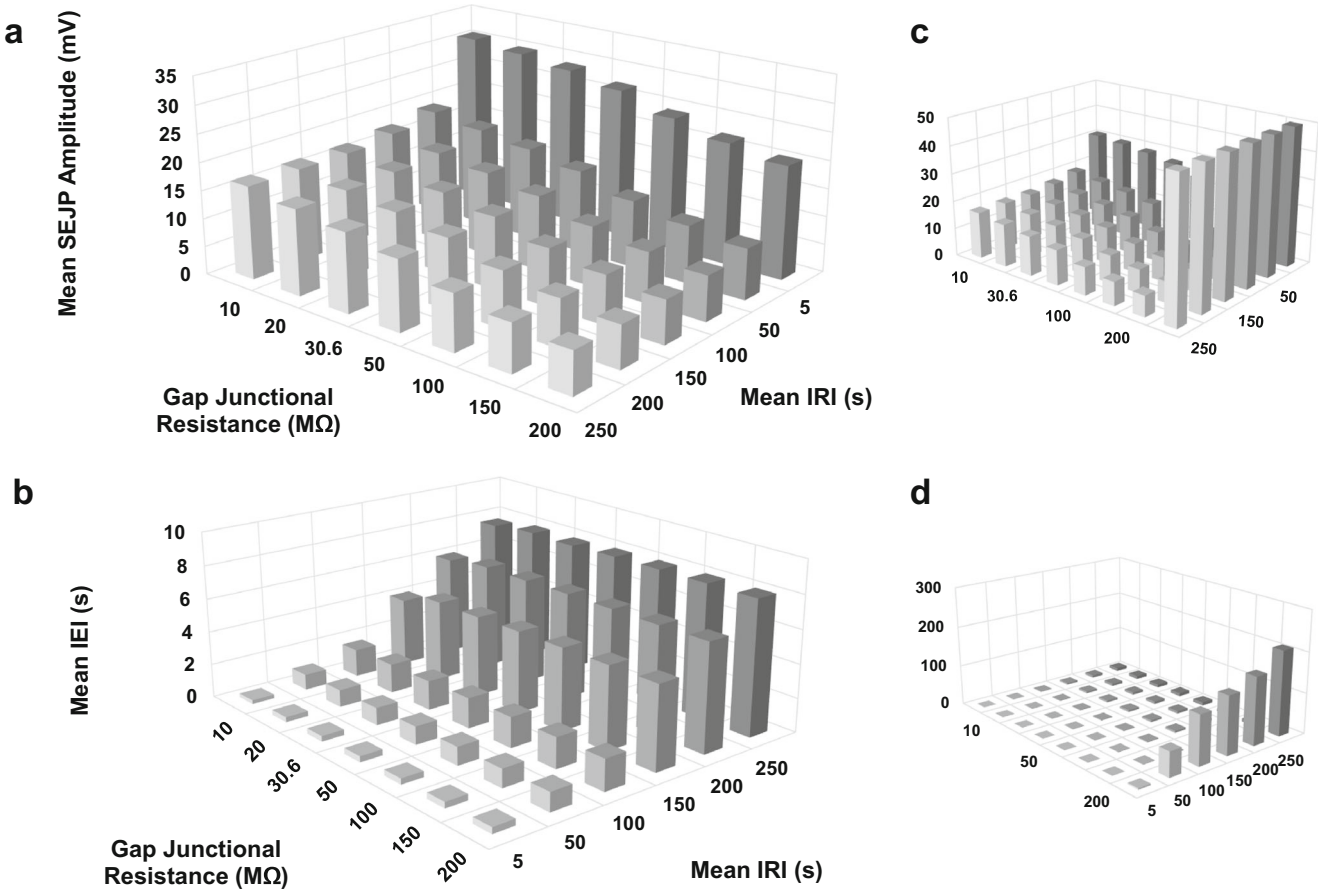

Fig. 11 Composite effect of coupling strength and mean IRI on (**a**) mean SEJP amplitude, and (**b**) mean IEI. (**c**) and (**d**) are modified versions of (a) and (b) respectively, incorporating gap junctional resistance of 74 GΩ. This very large value of gap junctional resistance (mimicking electrical isolation of the cells) leads to the very high observed values of mean SEJP amplitudes and IEI, dwarfing the values presented in (a) and (b)

2. Cell from unaffected region with augmented innervation: AugInn-A
3. Cell from denervated region (unaffected region has regular innervation): Patchy-B
4. Cell from denervated region (unaffected region has augmented innervation): AugInn-B
5. Cell from borderline region (unaffected region has regular innervation): Patchy-C
6. Cell from borderline region (unaffected region has augmented innervation): AugInn-C

Since it is conceivable that the pattern of denervation is spatially random rather than confined to a discrete region, we also simulated the scenario of random denervation. Unlike patchy denervation where denervation is localized in a patch, in this case random cells across the bundle lose NMJs. Thus for each degree of denervation, we explored two additional cellular microenvironments, namely:

7. Centroidal cell in case of random denervation – Random
8. Centroidal cell in case of random denervation (unaffected cells with augmented innervation) - AugRandom

As before, "control" innervation in our study corresponds to 100% innervation.

Figure 12a displays the effects of both patchy and random denervation, as well as of denervation with augmented innervation in the unaffected region. These effects are shown on mean SEJP amplitude under different conditions. Patchy denervation affects the electrical function of a closely placed cell (Patchy-B) to a greater extent as opposed to a cell located in a distant region (Patchy-A), unaffected by denervation. The cell in the borderline region (Patchy-C) is affected moderately. Consequently, irrespective of the degree of denervation, mean SEJP amplitude recorded at the Patchy-A cell remains almost unaffected (suffering only about 1.6% reduction). In contrast, mean SEJP amplitude recorded at the Patchy-B cell diminishes to a much greater extent as denervation progresses (diminished by 6.76% when remaining innervation is 50% of control, and by 9.74% when remaining innervation is 25%). Furthermore, when innervation density in the unaffected region increases, similar observations can be made between cell locations AugInn-A (in the unaffected region with augmented innervation) and AugInn-B (in the patchily denervated region) and AugInn-C (in the borderline region).

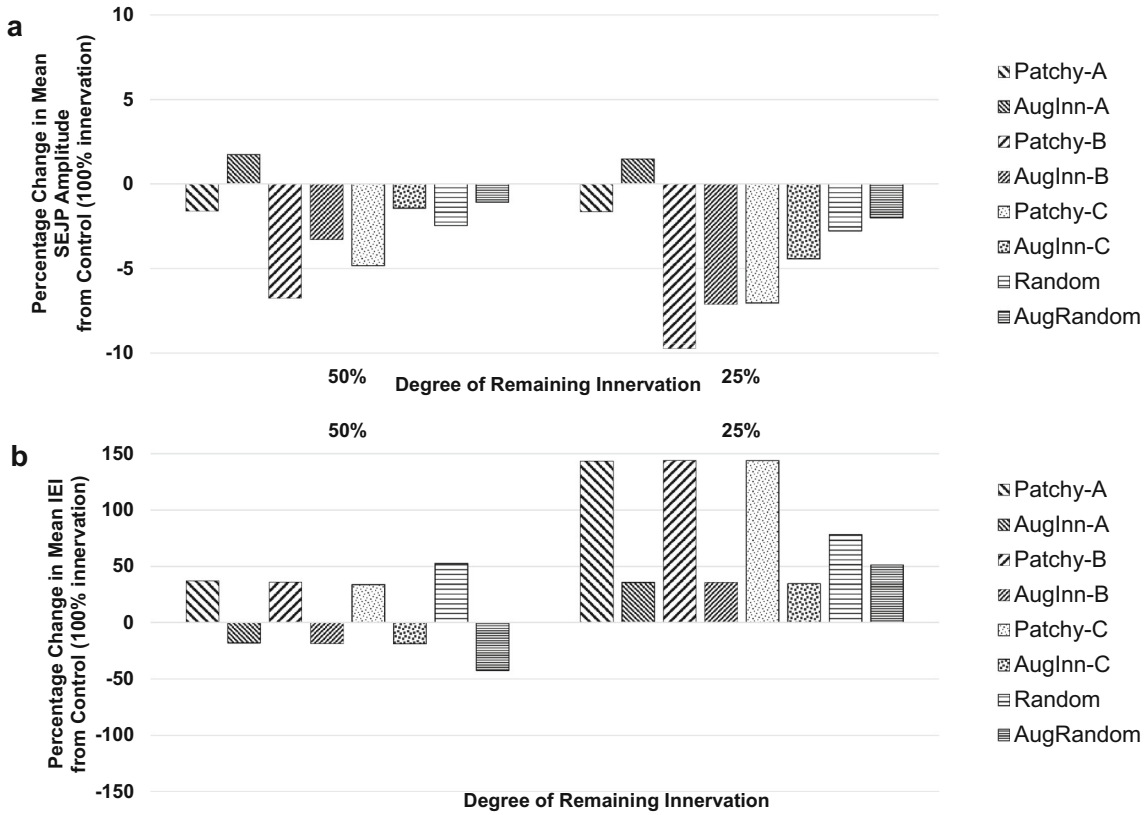

Fig. 12 Effect of patchy and random denervation and of denervation with augmented innervation on (**a**) mean SEJP amplitude, and (**b**) mean IEI

Figure 12b presents the effect of both patchy and random denervation, as well as of denervation with augmented innervation in the unaffected region. The effect is shown on mean IEI, for cells located in differing environments ('A' in the unaffected, 'B' in the denervated and 'C' in the borderline region). Denervation enhances the mean IEI irrespective of denervation type and cell location (increased by about 36% when remaining innervation is 50% of control, and by 144% when remaining innervation is 25%). Also, patchy denervation with augmented innervation in the unaffected zone reduces the mean IEI of spatio-temporal integration irrespective of the recording cell's location in the bundle. Differences in spatio-temporal integration of SEJPs were observed in case of random denervation as compared to patchy denervation, in spite of the same overall degree of denervation.

3.9 Pilot active bundle studies

Using the innervated model of the detrusor bundle we explored factors affecting spatio-temporal integration of neurotransmission-elicited passive electrical signals (SEJPs) in the smooth muscle syncytium. Consequently, active ion channels were not incorporated in the model. However, in order to corroborate the predictions arising from our passive model as to the implications for electrical excitability and contractile function, we carried out preliminary studies involving detrusor specific active ion channels (see Methods), so as to study the effects on spike generation and propagation.

Using this active model, we investigated the effect of parameters such as strength of cell-to-cell coupling, density of innervation and mean IRI on sAP generation within the detrusor bundle. Protocols for the simulations were identical to those employed for sub-threshold studies.

Figure 13a displays that as the gap junctional resistance increases from 10 MΩ to 20 MΩ, mean interval between sAPs falls drastically. However, with further increase in gap junctional resistance, no appreciable change is observed in mean inter-sAP interval. When gap junctional resistance is elevated to 20 times the input resistance of a single detrusor cell, *i.e.* to 74 GΩ (inset), inter-sAP interval is extremely high (~257 s).

Figure 13b shows that while there is significant reduction in mean inter-sAP interval as the innervation density increases from 10% to 100%, beyond the latter value (which is the default value), the change in mean inter-sAP interval is negligible.

Figure 13c displays that with increase in mean IRI mean inter-sAP interval increases. This observation was in accordance with the observation from the passive model.

A denervation study was carried out using the same protocol as outlined previously, with the inclusion of active ion channels. The conclusions from the passive study seemed to

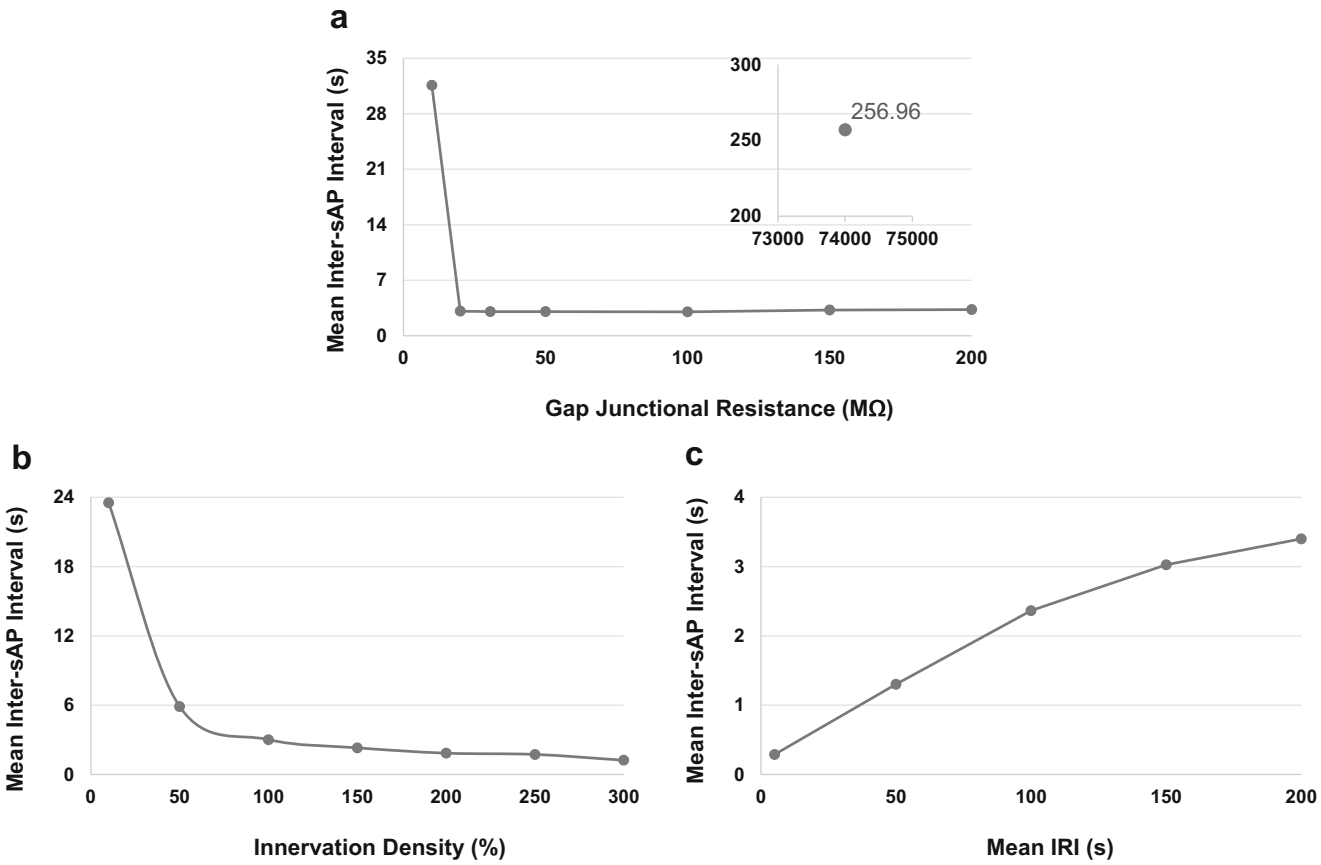

Fig. 13 Effect on sAP occurrence frequency of (**a**) coupling strength, (**b**) innervation density, and (**c**) mean IRI. Inset graph in (a) shows value for 74 GΩ gap junctional resistance (mimicking electrical isolation of the cells)

hold true in this case as well, as presented in Fig. 14. Denervation, be it patchy or random, significantly reduced the probability of sAP generation, thus increasing mean inter-sAP interval and the amount of change was dependent on degree of denervation. Also, with augmented innervation in the unaffected zone, in spite of denervation, sAP generation probability was enhanced, as evident by the reduced mean inter-sAP interval for AugInn and AugRandom cells. The recording location, *i.e.* whether it was the denervated or the unaffected zone, did not affect the observations.

4 Discussion

The work presented in this paper focuses on understanding the spread of spontaneous post-junctional potentials, particularly the

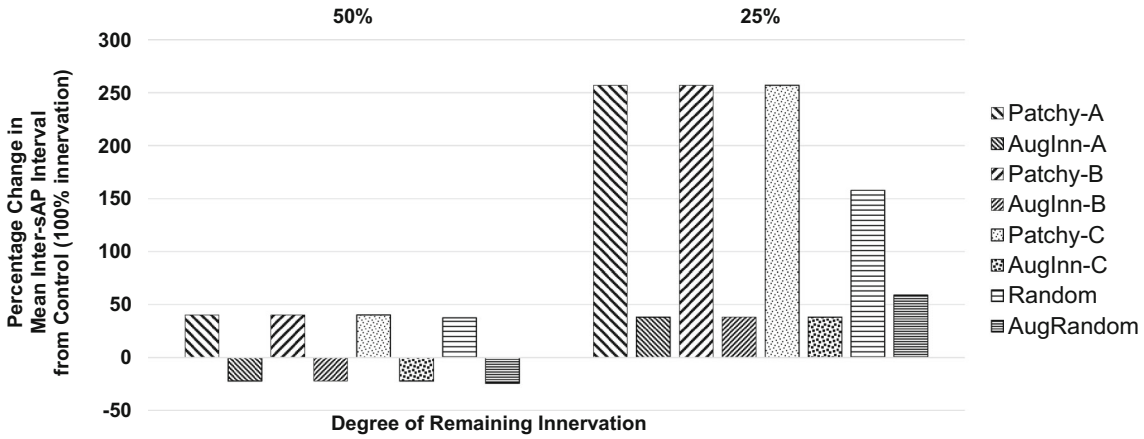

Fig. 14 Effect of patchy and random denervation and of denervation with augmented innervation on sAP generation

SEJPs, in the detrusor syncytium. Towards this end we have used the compartmental modelling technique offered by the NEURON simulation platform. Prior work utilizing NEURON to realize smooth muscle models has been limited to exploring syncytial properties, without taking spatio-temporal neurotransmission into account (single-layer model, Crane et al. 2001; three-dimensional model, Appukuttan et al. 2015). The novelty of the work presented here lies in modelling physiologically realistic spatially and temporally distributed synaptic inputs, with release features constrained by available physiological data, supplying a three-dimensional network of smooth muscle cells. Utilizing NEURON's event based modelling approach, we mimicked stochastic random neurotransmitter release within a smooth muscle bundle and thereby explored key aspects of spatio-temporal integration of post-junctional potentials in the detrusor. Using our model, we carried out studies of the kind that are best performed in the computational domain when currently available experimental techniques are inadequate for them, namely: (i) answering physiological questions pertaining to altered electrical response of the detrusor in pathology involving denervation; (ii) hypothesis testing with regard to counter-intuitive observations from location-dependent electrical activity in the tissue; (iii) making heuristic predictions, such as in relation to the implications of enhanced spontaneous release in pathological conditions, such predictions being amenable to experimental validation in the near future. We discuss below the observations made using our model, our deductions, the model's limitations and possible future enhancements to the model.

4.1 Spatio-temporal integration

Spatio-temporal integration of signals has been of much interest in the analysis of the dynamics of neuronal networks, and of the integration of signals within individual neurons, especially the funneling of signals from neuronal dendritic arbors into neuronal somata. Extensive studies have been done on the properties of information processing in individual neurons, such properties governed by their diverse dendritic morphologies and the varied volleys of spatio-temporally distributed synaptic inputs they receive. A major focus of such investigations, both experimental and computational, has been to examine integration of sub-threshold synaptic potentials in the somata, which is the primary site of information integration in neurons. The study of passive potentials and their spread and interaction has led to interesting observations and paved the way towards understanding the factors that determine action potential generation and, more broadly, modes of neuronal operation (Cash and Yuste 1998; Poirazi et al. 2003).

Any cell in an innervated syncytial smooth muscle network, such as the detrusor, collates subthreshold junction potentials analogous to the way in which somata of neurons receive passive synaptic potentials from their dendritic branches. Spatio-temporal integration of junction potentials in smooth muscles is critical to the electrical and subsequent mechanical function of the tissue. However, no fine-grained studies have so far been conducted on the details of spatio-temporal integration of SEJPs. Using our model and drawing a parallel with synaptic potential integration in neurons, we explored the mode of summation of passive SEJPs in the detrusor cellular network.

Our observations suggest that integration of sub-threshold signals in the detrusor is essentially sub-linear (Fig. 3). Furthermore, the percentage linearity depends on the relative positions of cells in which the individual SEJPs are elicited. For example, when superimposing SEJPs were elicited within the same cell (Case I) the summated response was poorest in strength. Given the first SEJP, the electro-chemical driving force for the second SEJP within the same cell is lowered, which accounts for the observation. If we consider the propagation path for an SEJP along the syncytium through cells and interconnecting gap junctions, Vertex 8 is farthest away from Vertex 1 (diagonally opposite ends of the bundle, Fig. 1). Also Vertex 2 is farther away from Vertex 1 as compared to Vertex 3, given the dimensions of a detrusor cell (200 μm in length and 6 μm in diameter). It follows that an SEJP elicited in Vertex 1 will affect the electrochemical driving force in Vertex 3 to a greater extent than in Vertex 2 and *vice versa*. Thus, the integrated signal will have a smaller amplitude if the NMJs are in Vertex 1 and Vertex 3 (Case II) as compared to the case when NMJs are in Vertex 1 and Vertex 2 (Case IV). In Case III, the second NMJ was present on the centroidal cell. Thus, the distance between two NMJs in this case was greater than in Case II. The reduced percentage linearity in Case III (also evident in Fig. 3b, cell 222), as compared to Case II (Fig. 3b, cell 040) was thus counterintuitive. We conjectured that such an observation might arise because in Case III one of the NMJs was on the cell being recorded from (cell 222). This would lead to recording an un-attenuated, very high amplitude SEJP. Consequently, the algebraic sum of individual SEJP amplitudes would be relatively higher, thus lowering the calculated percentage linearity. We verified our conjecture from the individual SEJP amplitudes recorded.

4.2 Effects of individual parameters

The three-dimensional detrusor-bundle model with synaptic drive is a complex layout with several parameters governing the characteristics of spatio-temporal integration. While many of these are bound to affect the electrical properties of the syncytium, some of them are major players not just from a theoretical but from a physiological perspective as well, which we discuss below. Since the object of this work was to understand spatio-temporal integration of SEJPs, we looked at mean SEJP amplitude (mV) and mean IEI (s) recorded from a cell in the syncytium, as outcome measures (see Methods). Theoretical predictions can be made as to the effects of key

parameters on these outcome measures, and provide benchmarks against which to test the robustness of our model. These are discussed below in relation to the corresponding results.

Syncytium size The size of a syncytium influences its electrical response (Sourav and Manchanda 2000; Sengupta et al. 2018). Previous studies have shown how with increase in the size of a syncytium (number of cells participating in the connected network), the input resistance as measured in any individual cell falls (Appukuttan et al. 2015). This occurs due to the incorporation of progressively greater gap-junctional connectivity, which forms low resistance shunts compared to the high membrane resistance. Consequently the apparent resistance offered to any input current (in this case, junction current through the neurotransmitter-gated receptors) is reduced. Previous studies (Appukuttan et al. 2015) looked at this effect solely on stand-alone SEJPs. We observed that as syncytium size was enhanced, mean SEJP amplitude underwent a similar reduction during spatio-temporal integration (STI) of SEJPs (Fig. 4a). The reduction in this case was however more pronounced than in case of stand-alone SEJPs. This may be explained as follows. As a greater number of cells are incorporated in the network, input resistance is progressively lowered (Fig. 4c). Consequently, the amplitude of individual SEJPs at the cell of origin in the syncytium falls, as was observed in case of stand-alone SEJPs. However to add on to this effect, in the case of spatio-temporal integration the SEJPs propagating from distant cells traverse a greater distance with rise in syncytium size and get attenuated more severely on their passage to the recording site. Thus, in spite of possible superposition during spatio-temporal integration, the mean SEJP amplitude was reduced with increase in syncytium size.

Experimental intracellular recordings from detrusor smooth muscle cells have never reported the size of the bundle (which is different from the tissue preparation size), from which recordings have been obtained. Within the tissue prepared for intracellular recordings (about 2 by 10 mm, Bramich and Brading 1996), several finite bundled sub-syncytia (sub-millimeter dimensions) are likely to be present. The computational model used previously to investigate sub-threshold electrical activity in the detrusor smooth muscle was not endowed with synaptic drive (Appukuttan et al. 2015). Consequently, there have been no reports as yet pertaining to the effect of syncytium size on mean IEI recorded from any cell in the syncytium. The prime feature of our model was the incorporation of stochastic synaptic drive within the smooth muscle grid. This enabled us to mimic spontaneous SEJPs occurring randomly in time as well as distributed randomly in space throughout the syncytium. Figure 4b shows that with increase in size of syncytium, the mean IEI (mean interval between SEJPs recorded from a cell) diminished. During this study, the density of innervation was held constant and so was mean frequency of release at each NMJ. Consequently, with rise in syncytium size, the number of NMJs increases while the mean interval between subsequent releases at any given NMJ remains the same. This leads to an enhancement in the number of SEJPs with increase in syncytium size, within a given window of observation, consequently reducing mean IEI.

Within the detrusor, bundles of smooth muscle cells form sub-syncytia of varied sizes and these sub-syncytia are coordinated during voiding by means of nerve-evoked motor response (Bramich and Brading 1996). The varied sizes of syncytia allow for discrete focal contractions during the filling phase. These result in micromotions (Meng et al. 2008; Drake et al. 2017) which help to maintain compliance. Our findings point to a correlation between the size of such an electrical network and emergent electrical properties of integrated signals (such as mean SEJP amplitude and mean IEI). An implication of this correlation is that experimental recordings from different parts of tissue strip preparations may be analyzed with these observations in mind, which may aid in the qualitative estimation of network sizes from which recordings are made within the same tissue. For example, a recording that has lower mean SEJP amplitude along with lower mean IEI compared to another recording is likely to have been made from a bigger bundle, while a recording from a smaller bundle will display higher mean SEJP amplitude and greater mean IEI.

Coupling strength In a well-coupled syncytium, where the gap-junctional resistance is relatively low, signals such as SEJPs can easily propagate from their sites of origin to coupled neighbours with minimal attenuation. In contrast, these signals get attenuated more heavily while propagating in a poorly coupled syncytium, owing to higher gap-junctional resistances.

Studies pertaining to the effect of gap-junctional resistance, which is a measure of coupling strength, on passive electrical properties of detrusor syncytium have shown that the input resistance of the tissue rises with increase in gap-junctional resistance (Palani et al. 2006). Consequently, in a syncytium where cells are connected by gap junctions offering higher resistances, a passive signal such as SEJP is expected to exhibit higher amplitude. However our observation in this regard was contradictory to expectation. In Fig. 5c we observe that with increase in gap junctional resistance, mean SEJP amplitude reduces, except for the case where gap junctional resistance was as high as 74 GΩ (20 times the input resistance of a single detrusor cell). We propose it is the dual effect of gap junctional resistance, in the context of spatio-temporal integration of signals, which lead to such an observation. With a raised value of gap-junctional resistance, the SEJP elicited in any individual cell attains higher amplitude. Also with such reduced coupling strength, SEJPs propagating from distant cells get heavily attenuated, leading to a decrease in the mean SEJP amplitude. Such a dual effect of coupling strength on elicited and propagated SEJPs was explored using our model as well.

Figure 15 depicts that with diminished coupling between cells, the amplitude of SEJPs elicited at any given cell was boosted while a propagated SEJP got attenuated. When the coupling almost ceased to exist (as observed with gap junctional resistance of 74 GΩ in Fig. 5b) the elicited SEJPs were almost 50 mV in amplitude, but they failed to propagate. With such a high value of gap junctional resistance, the cells are effectively electrically isolated and the observed SEJPs in that case are only those that elicited within the cell being recorded from. Such high SEJP amplitude, it must be noted here, is limited by the reversal potential of the NMJ (0 mV). Given our observation in Fig. 5c, the effect of attenuation due to propagation through gap junctions was greater than the effect of increased amplitude of stand-alone elicited SEJPs (at respective sources of origin). This can however be explained from observations made in an earlier study which stated that in a three-dimensional 5*5*5 detrusor syncytium (with 125 cells), dependence of input resistance on gap-junctional resistance is low (Appukuttan et al. 2015). Also, cumulative effect of propagated SEJPs was more than that of elicited SEJPs.

Experimental studies altering strength of coupling utilizing putative gap-junction blockers such as heptanol report changes in electrical properties such as input resistance (Palani and Manchanda 2006). However, effect of such blockers on IEI of SEJPs has not been reported, either experimentally or computationally. We observed, as in Fig. 5d that with rise in gap-junctional resistance mean IEI remained almost invariant.

The strength of coupling between cells in a syncytium can thus affect its electrical functioning, in particular the amplitude of recorded events. This will have direct implications for the generation of supra-threshold signals, *i.e.* the spontaneous action potentials (sAPs) which are critical for the generation of focal contractions. We conjectured that since poorer intercellular coupling leads to higher amplitude of elicited SEJPs, it should increase the probability of membrane potential exceeding threshold to elicit sAPs. This was corroborated by inclusion of active ion channels in the model (Fig. 13a). Reduction in mean inter-sAP interval with an enhancement in gap-junctional resistance suggested a rise in the number of sAPs generated during the recording period. However, we also observed that beyond the control value of 30.6 MΩ, further increase in gap junction resistance seemed to have no effect on sAP generation. It must be noted that such enhancement will still influence the amplitude of propagated SEJPs, thus influencing spatio-temporal integration. The relatively higher value of inter-sAP interval at 10 MΩ was ascertained to be due to generation of fewer sAPs owing to lower input resistance. In addition, at 74 GΩ, the cells were electrically isolated from each other and sAPs could be recorded only from one cell, resulting in a lower number of sAPs and consequently very high inter-sAP interval.

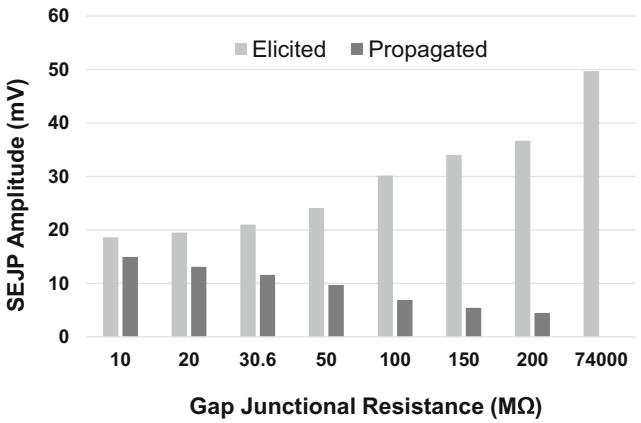

Fig. 15 Dual effect of coupling strength: increase in amplitude of elicited SEJP and decrease in amplitude of propagated SEJP with increase in gap junctional resistance

Innervation density The detrusor receives a distributed innervation (Gabella 2012). Specific electrophysiological studies correlating density of innervation to electrical activity of the tissue are scant. No computational investigation pertaining to varying degrees of innervation and the effects thereof on detrusor electrophysiology has been conducted either. However, histological studies have correlated detrusor instability with altered innervation observed in the tissue samples (Brading 2005).

Since the incorporation of distributed NMJs is a key feature of our model, we studied the effect of varying degrees of innervation on synaptic drive of the detrusor. We observed a steady increase of mean SEJP amplitude with increase in density of innervation (Fig. 6b). With the total number of cells in the syncytium remaining constant, as a greater fraction of cells receive NMJs, a larger number of SEJPs are elicited across the syncytium, leading in turn to elevated probability of superposition during spatio-temporal integration. We therefore observe a higher mean amplitude of SEJP, which is in accord with theoretical and experimental expectations.

Also on account of augmented occurrence of SEJPs across the syncytium with greater innervation density, the mean interval between any two successive SEJPs is reduced. This is evident in Fig. 6c, where with rising innervation density, mean IEI between SEJPs declines. Akin to the situation with elevated mean SEJP amplitude, reduced mean IEI heightens the probability of the membrane potential exceeding sAP threshold since a decrement in mean IEI enhances the probability of superposition of adjoining SEJPs. Such an effect should result in larger number of sAPs generated and as a consequence, should lead to an enhanced occurrence of focal contractions. This possibility was explored by inclusion of active ion channels in our model. We observed in Fig. 13b that the denser the innervation, the lower the mean inter-sAP interval, suggesting enhanced probability of sAP generation.

Mean inter-release interval A salient attribute of SEJPs is the temporal stochasticity of their occurrence, resulting from stochastic release of neurotransmitter from innervating varicosities. Studies on the temporal characteristics of such spontaneous release events are scarce. We wished to explore if and how a change in release frequency affects the electrical activity of the detrusor.

Figure 7b shows that as the mean IRI increases (release frequency decreases), mean SEJP amplitude reduces. Physiologically this would reduce the probability of sAP generation. This might result in the bladder wall failing to be compliant. On the other hand, an increase in this release frequency will result in a heightened probability of sAP generation thus leading to heightened focal contractions. This could be a probable cause for incontinence. In Fig. 7c we observe that with greater mean IRI at NMJs, there is elevation in mean IEI between SEJPs. Consequently, pathological conditions may be explained in terms of mean IEI as well. α-Latrotoxin is known to facilitate release of neurotransmitter from varicosities of nerve terminals. A dose dependent study of such a drug, influencing the electrical outcome from the muscle could be carried out, which could assist in controlling abnormalities arising out of anomalous spontaneous release frequency from NMJs. Computational models may also explore the effect that such frequency of release will exert on the generation of sAPs. We incorporated active ion channels in our model to address this question. Figure 13c suggests that as the spontaneous release from any varicosity becomes less frequent, probability of sAP generation diminishes which is reflected as a higher mean inter-sAP interval within a recording duration.

Recording location Electrical coupling between cells, which facilitates propagation of electrical signals within a network, endows a syncytium with atypical electrical characteristics (Manchanda 1995). Besides the size of a syncytium or the strength of inter-cellular coupling within it, the location of cells within a syncytium influences the spatio-temporal integration of signals in individual cells. This is because a cell's location (such as at the vertex or embedded at the core of the network) defines its biophysical microenvironment. Microscopically-visualized location-specific intracellular recordings from the detrusor have not been reported yet. Our model makes certain predictions that could be tested using directed electrophysiological recordings.

When we explored different microenvironments of recorded cells in terms of position within the bundle, no significant difference was observed between mean SEJP amplitudes recorded from a vertex cell and a centroidal cell. Furthermore, the maximum amplitudes of SEJPs recorded in each case were nearly equal (Fig. 8a). The maximum amplitudes recorded in each cell correspond to those SEJPs that propagate the least and thus suffer minimal attenuation; essentially SEJPs elicited in close proximity to the cell being recorded from. Such observations are expected in a relatively small syncytium, where an SEJP arising at any cell can propagate to any connected neighbour without significant attenuation. The mean IEIs recorded at these two cells were not significantly different either, as observed in Fig. 8b.

However, previous studies have reported that location within a bundle may significantly influence the characteristics of signals in the syncytium (Appukuttan et al. 2015). We conjectured that syncytium size may be a modulating factor in such dependence. The finding presented in Fig. 8c corroborates this conjecture, since with increase in syncytium size the ratio of mean SEJP amplitudes, recorded from the vertex cell and the corresponding centroidal cell, increased progressively. In a larger syncytium (such as 15^3), the core or centroid cell has greater number of connected neighbours along all axes, thus surrounding it with a greater electrical sink. Hence charge build up is less as compared to its corresponding edge or vertex cell. This discrepancy diminishes with reduction in number of cells in the syncytial network (such as 5^3). Thus in bigger bundles, there is a higher probability of sAP generation along the edges; these sAPs may then propagate across the bundle. Experimental studies corroborate this notion, as sAPs have been reported to originate along edges and then propagate across the bundles (Hashitani et al. 2001).

4.3 Composite effects

Studying the effects of a suite of key parameters on spatio-temporal integration of SEJPs in detrusor syncytium had helped us further validate the model by being able to interpret the model outcomes in the light of theoretical predictions or prior experimental observations. Having tested the model, we wished to examine relative sensitivity of elicited signals to certain central parameters such as gap junctional resistance, density of innervation and inter-release interval at an NMJ. In essence we wished to assess at a qualitative level the question: to which model parameter(s) are the characteristics of spatio-temporal integration (such as the mean SEJP amplitude and the mean IEI) most sensitive?

Taken together, the observations from Figs. 9a, 10a and 11a indicate that mean SEJP amplitude is most sensitive to strength of inter-cellular coupling within a bundle. Likewise, collated observations from Figs. 9b, 10b and 11b imply that while mean IEI varies most strongly with density of innervation, strength of coupling affects it negligibly. For the extreme case of gap junctional resistance being 20-fold the input resistance of single detrusor cell (74 GΩ), the observations were atypical and outliers. Hence the composite figures have been modified after inclusion of this condition (Fig. 10c–d). Irrespective of innervation density or mean IRI, when the cells are isolated from each other there is no spatial integration of signals. In such a scenario, only the SEJPs arising in the cell being recorded from can be observed. Hence, for 10% innervation density no SEJP was observed when gap junctional resistance was 74 GΩ. For higher innervation densities, when

the cell being recorded from was endowed with NMJ(s), high mean SEJP amplitude (Fig. 10c) was observed and mean IEI depended solely on signals arising within the recorded cell (Fig. 10d).

Comparative experimental studies on SEJP biophysics of detrusor smooth muscle do not exist, but they do for another smooth muscle tissue, the vas deferens. Amplitude as well as frequency of SEJP occurrence is higher in rat vas deferens. Thus, mean IEI is lower in rat vas deferens, which can be attributed to a relatively high density of innervation in this tissue (Goto et al. 1977). Also, it has been reported that electrical coupling between smooth muscle cells of guinea-pig vas deferens is better than in rat. In the absence of targeted comparative studies on rat and guinea-pig detrusor, the vas deferens (another bundled syncytial smooth muscle) offers the closest approximation. From our studies on the detrusor model we speculate that higher recorded SEJP amplitudes would correspond to relatively poor intercellular coupling between cells and/or dense innervation. The histological observations of rat vas deferens being less well coupled and more densely innervated than guinea-pig vas, together with electrophysiological observations of higher SEJP amplitudes from rat vas, are congruent with our model outcomes. Also, our model suggests that mean IEI is sensitive to innervation density, which is in accord with experimental observations made in the vas.

4.4 Study on denervation

Owing to our incomplete understanding of normal bladder functioning, several features of bladder pathophysiology remain obscure. A pathophysiological condition of the detrusor characterized by denervation of the tissue in patches has been reported based on histological observations (Brading 2005). However, corresponding electrophysiological observations have not been reported. Consequently, structure-function complementarity in diseased conditions remains unaddressed. As a result, electrical interventions for therapy lack specificity and efficacy. This prompted us to utilize our model to simulate the condition of patchy denervation and test hypotheses pertaining to possible changes that might result in the observed electrical behaviour.

We observed that with exacerbation in the extent of denervation, the mean SEJP amplitude diminishes correspondingly (Fig. 12a). A cell which is in a patchily denervated zone (Patchy-B) exhibits lower amplitude SEJPs, as against a cell in an unaffected zone (Patchy-A), within the same bundle. However, in case of mean IEI, the effect is global (Fig. 12b). Irrespective of the location of the cell (in the denervated or unaffected zone) the mean IEI increases. This differential effect on mean SEJP amplitude and mean IEI can be explained from the previous discussion on composite effects where we observe that innervation density strongly influences mean IEI. Patchy denervation can thus reduce the excitability of a bundle. This prediction was tested by the inclusion of active ion channels in the model, where we found that in a denervated bundle inter-sAP interval is enhanced and this effect worsens with greater severity of denervation (Fig. 14). Thus, within a bundle, an affected patch may be more likely to fail in initiating a contraction. This in turn is likely to disrupt the existent synergy of micromotions under physiological conditions.

Imaging studies also indicate an increase in the innervation of unaffected regions in patchily denervated detrusor tissue (Brading 2005). This is possibly a compensatory mechanism wherein, the tissue tries to compensate for the loss in NMJs in the denervated patches by way of augmented innervation in the other regions. Using our model we tested this prediction (Figs. 12 and 14). Our results suggest that augmented innervation is likely to enhance the possibility of sAP generation, thereby aiding in regaining synergy of contractions.

4.5 Limitations

We developed the model reported here in view of the focus of our investigation, the fundamental idea being to build an in-silico detrusor smooth muscle bundle receiving distributed stochastic synaptic inputs. Since the focus was on the continence phase of bladder function, the model was restricted to a single bundle which is an electrically isolated syncytium in the detrusor tissue. Studying coordination of multiple such bundles under evoked motor nerve response during voiding can be addressed in a more elaborate model. Also, as we were interested in studying the spatio-temporal integration of synaptic potentials in the smooth muscle, a detailed model of vesicular release of neurotransmitters from varicosities and the dynamics of their attachment to muscle cell receptors was not undertaken. Instead, the focus was on temporal kinetics of random release, which was successfully implemented (see Methods). Reports pertaining to structural details of the detrusor are scarce. Therefore, we chose to set out with a simple model in terms of homogenous strength of coupling throughout the bundle. Also, quantitative estimates of innervation density, release frequency, and quantum of release being unknown, the model had to be subjected to extensive tuning during its validation against experimental observations in terms of outcome measures (such as SEJP amplitude distribution, IEI histogram). Furthermore, since our object was the study of network level properties, subcellular mechanisms such as calcium dynamics were simplified. Lastly, our focus has been the study of subthreshold events or SEJPs, with a view to investigate spatio-temporal integration of synaptic potentials. Hence active ion channels were incorporated only for preliminary studies so as to repose confidence in our observations made from the passive model. This helped us in

limiting complexity in an already large parameter space. The detrusor has a large set of active ion channels and studying in detail the properties of action potential propagation in a detrusor bundle merits a separate study. Having understood the functioning of a detrusor bundle in the passive domain through our model, more extensive investigations involving active ion channels may be conducted in future to explore spread of active signals.

4.6 Conclusions

In summary, we have presented here the development and validation of an innervated syncytial bundle model of the detrusor. Using this model we explored interactive effects of key parameters in modulating spatio-temporal integration of sub-threshold potentials in the detrusor. Our simulations have given rise to interesting observations pertaining to spontaneous neurotransmitter release frequency, innervation density and coupling strength in detrusor smooth muscle, which provide pointers to future experimental studies. Investigations to ascertain the role of spontaneous release in signal integration merits attention, such data being scarce. Experiments probing the effects of innervation density, involving the manipulation of recruitment of varicosities, may be technically challenging. Experimental studies, however, may possibly be designed that make use of the drug α-Latrotoxin to alter release frequency from varicosities and study the effects thereof. Such experimental studies could test predictions from our computational work. Observations from our model also prompted us to revise certain notions of spatio-temporal integration, for instance with regard to the part played by the microenvironment of a cell in bundle in modulating its electrical activity, our observations were counter-intuitive. We proposed an explanation for such apparent contradiction and with the aid of further tests, we verified our explanation. We have also used our model to predict probable changes in tissue electrophysiology in a well-defined, previously reported disease condition. Our model offers the possibility of exploration of other pathologies as well (particularly those characterized by changes of neurotransmission at cellular or network levels). With suitable adjustments in parameters and other alterations as necessary, it can also be used to address such questions in other innervated syncytial tissues.

Acknowledgements The work was supported by grants from the Department of Biotechnology (DBT), India (BT/PR12973/MED/122/47/2016) and the UK-India Education and Research Initiative, UKIERI (UKUTP20110055).

Compliance with ethical standards

Conflict of interest None.

References

Andersson, K. E., Chapple, C., & Wein, A. (2001). The basis for drug treatment of the overactive bladder. *World Journal of Urology, 19*(5), 294–298.

Appukuttan, S., Brain, K. L., & Manchanda, R. (2015). A computational model of urinary bladder smooth muscle syncytium. *Journal of Computational Neuroscience, 38*(1), 167–187.

Bennett, M. R. (1973). Structure and electrical properties of the autonomic neuromuscular junction. *Philosophical Transactions of the Royal Society of London. B, Biological Sciences, 265*(867), 25–34.

Brading, A. F. (1997). A myogenic basis for the overactive bladder. *Urology, 50*(6), 57–67.

Brading, A. F. (2005). Overactive bladder: Why it occurs. *Women's Health Medicine, 2*(6), 20–23.

Bramich, N. J., & Brading, A. F. (1996). Electrical properties of smooth muscle in the Guinea-pig urinary bladder. *The Journal of Physiology, 492*(1), 185–198.

Cash, S., & Yuste, R. (1998). Input summation by cultured pyramidal neurons is linear and position-independent. *Journal of Neuroscience, 18*(1), 10–15.

Cash, S., & Yuste, R. (1999). Linear summation of excitatory inputs by CA1 pyramidal neurons. *Neuron, 22*(2), 383–394.

Crane, G. J., Hines, M. L., & Neild, T. O. (2001). Simulating the spread of membrane potential changes in arteriolar networks. *Microcirculation, 8*(1), 33–43.

Drake, M. J., Gardner, B. P., & Brading, A. F. (2003). Innervation of the detrusor muscle bundle in neurogenic detrusor overactivity. *BJU International, 91*(7), 702–710.

Drake, M. J., Kanai, A., Bijos, D. A., Ikeda, Y., Zabbarova, I., Vahabi, B., & Fry, C. H. (2017). The potential role of unregulated autonomous bladder micromotions in urinary storage and voiding dysfunction; overactive bladder and detrusor underactivity. *BJU International, 119*(1), 22–29.

Fry, C. H., Cooklin, M., Birns, J., & Mundy, A. R. (1999). Measurement of intercellular electrical coupling in Guinea-pig detrusor smooth muscle. *The Journal of Urology, 161*(2), 660–664.

Fry, C. H., Sui, G. P., Severs, N. J., & Wu, C. (2004). Spontaneous activity and electrical coupling in human detrusor smooth muscle: Implications for detrusor overactivity*? Urology, 63*(3), 3–10.

Gabella, G. (1995). The structural relations between nerve fibres and muscle cells in the urinary bladder of the rat. *Journal of Neurocytology, 24*(3), 159–187.

Gabella, G. (2012). Cells of visceral smooth muscles. *Journal of Smooth Muscle Research, 48*(4), 65–95.

Goto, K., Millecchia, L. L., Westfall, D. P., & Fleming, W. W. (1977). A comparison of the electrical properties and morphological characteristics of the smooth muscle of the rat and Guinea-pig vas deferens. *Pflügers Archiv, 368*(3), 253–261.

Hashitani, H. B. N. J., Bramich, N. J., & Hirst, G. D. S. (2000). Mechanisms of excitatory neuromuscular transmission in the Guinea-pig urinary bladder. *The Journal of Physiology, 524*(2), 565–579.

Hashitani, H., Fukuta, H., Takano, H., Klemm, M. F., & Suzuki, H. (2001). Origin and propagation of spontaneous excitation in smooth muscle of the Guinea-pig urinary bladder. *The Journal of Physiology, 530*(2), 273–286.

Hashitani, H., Brading, A. F., & Suzuki, H. (2004a). Correlation between spontaneous electrical, calcium and mechanical activity in detrusor smooth muscle of the Guinea-pig bladder. *British Journal of Pharmacology, 141*(1), 183–193.

Hashitani, H., Yanai, Y., & Suzuki, H. (2004b). Role of interstitial cells and gap junctions in the transmission of spontaneous Ca2+ signals in detrusor smooth muscles of the Guinea-pig urinary bladder. *The Journal of Physiology, 559*(2), 567–581.

Hayase, M., Hashitani, H., Kohri, K., & Suzuki, H. (2009). Role of K+ channels in regulating spontaneous activity in detrusor smooth muscle in situ in the mouse bladder. *The Journal of Urology, 181*(5), 2355–2365.

Inoue, R., & Brading, A. F. (1990). The properties of the ATP-induced depolarization and current in single cells isolated from the Guinea-pig urinary bladder. *British Journal of Pharmacology, 100*(3), 619–625.

Johnston, L., Cunningham, R. M., Young, J. S., Fry, C. H., McMurray, G., Eccles, R., & McCloskey, K. D. (2012). Altered distribution of interstitial cells and innervation in the rat urinary bladder following spinal cord injury. *Journal of Cellular and Molecular Medicine, 16*(7), 1533–1543.

Krasnoperov, V. G., Bittner, M. A., Beavis, R., Kuang, Y., Salnikow, K. V., Chepurny, O. G., Little, A. R., Plotnikov, A. N., Wu, D., Holz, R. W., & Petrenko, A. G. (1997). α-Latrotoxin stimulates exocytosis by the interaction with a neuronal G-protein-coupled receptor. *Neuron, 18*(6), 925–937.

Mahapatra, C., Brain, K. L., & Manchanda, R. (2018). A biophysically constrained computational model of the action potential of mouse urinary bladder smooth muscle. *PLoS One, 13*(7), e0200712.

Manchanda, R. (1995). Membrane current and potential change during neurotransmission in smooth muscle. *Current Science, 69*(2), 140–150.

Manchanda, R., Appukuttan, S., & Padmakumar, M. (2019). Electrophysiology of syncytial smooth muscle. *Journal of Experimental Neuroscience, 13*, 1179069518821917.

Meng, E., Young, J. S., & Brading, A. F. (2008). Spontaneous activity of mouse detrusor smooth muscle and the effects of the urothelium. *Neurourology and Urodynamics: Official Journal of the International Continence Society, 27*(1), 79–87.

Neuhaus, J., Wolburg, H., Hermsdorf, T., Stolzenburg, J.-U., & Dorschner, W. (2002). Detrusor smooth muscle cells of the Guinea-pig are functionally coupled via gap junctions in situ and in cell culture. *Cell and Tissue Research, 309*(2), 301–311.

Padmakumar, M., Brain, K. L., Young, J. S., & Manchanda, R. (2018). A four-component model of the action potential in mouse detrusor smooth muscle cell. *PLoS One, 13*(1), e0190016.

Palani, D., & Manchanda, R. (2006). Effect of heptanol on noradrenaline-induced contractions in rat vas deferens. *Journal of Smooth Muscle Research, 42*(1), 49–61.

Palani, D., Ghildyal, P., & Manchanda, R. (2006). Effects of carbenoxolone on syncytial electrical properties and junction potentials of Guinea-pig vas deferens. *Naunyn-Schmiedeberg's Archives of Pharmacology, 374*(3), 207–214.

Poirazi, P., Brannon, T., & Mel, B. W. (2003). Arithmetic of subthreshold synaptic summation in a model CA1 pyramidal cell. *Neuron, 37*(6), 977–987.

Sengupta, N., Brain, K. L., & Manchanda, R. (2015, August). Spatiotemporal dynamics of synaptic drive in urinary bladder syncytium: A computational investigation. *In 2015 37th Annual International Conference of the IEEE Engineering in Medicine and Biology Society (EMBC)* (pp. 8074–8077). IEEE.

Sengupta, N., Brain, L. K., & Manchanda, R. (2018, July). Cellular Environment in a Bundle Modulates SEJP Characteristics in Detrusor Smooth Muscle. *In 2018 40th Annual International Conference of the IEEE Engineering in Medicine and Biology Society (EMBC)* (pp. 5842–5845). IEEE.

Sourav, S., & Manchanda, R. (2000). Influence of the size of syncytial units on synaptic potentials in smooth muscle. *Medical and Biological Engineering and Computing, 38*(3), 356–359.

Tomita, T. (1976). Electrophysiology of mammalian smooth muscle. *Progress in Biophysics and Molecular Biology, 30*, 185–203.

Wang, H. Z., Brink, P. R., & Christ, G. J. (2006). Gap junction channel activity in short-term cultured human detrusor myocyte cell pairs: Gating and unitary conductances. *American Journal of Physiology-Cell Physiology, 291*(6), C1366–C1376.

Wüst, M., Averbeck, B., Reif, S., Bräter, M., & Ravens, U. (2002). Different responses to drugs against overactive bladder in detrusor muscle of pig, Guinea pig and mouse. *European Journal of Pharmacology, 454*(1), 59–69.

Young, J. S., Brain, K. L., & Cunnane, T. C. (2007). The origin of the skewed amplitude distribution of spontaneous excitatory junction potentials in poorly coupled smooth muscle cells. *Neuroscience, 145*(1), 153–161.

Young, J. S., Meng, E., Cunnane, T. C., & Brain, K. L. (2008). Spontaneous purinergic neurotransmission in the mouse urinary bladder. *The Journal of Physiology, 586*(23), 5743–5755.